

ABSTRACT

GAVENKO, ROMAN. Investigating the Effects of Structural Changes to Enzymatic Activity in Isoenzymes of Dehaloperoxidase from *Amphitrite ornata*. (Under the direction of Dr. Reza A. Ghiladi).

Dehaloperoxidase (DHP) from the terebellid polychaete *Amphitrite ornata* is a coelomic enzyme that is capable of reversible oxygen binding, peroxidase activity and recently reported peroxygenase and oxidase activities. Two isoenzymes of DHP, A and B, are encoded by separate genes and are not alleles of a single gene. DHP B differs from DHP A by 5 amino acids (I9L, R32K, Y34N, N81S, and S91G) and exhibits a threefold increase in peroxidase activity and nearly a threefold increase in peroxygenase activity compared to DHP A.

DHP represents a truly unique enzyme due to its ability to perform a diverse range of functions. The flexibility of this heme enzyme comes at a cost of decreased catalytic activity and efficiency compared to specialized monofunctional counterparts. The unique nature of the DHP active site, which lacks the additional structural features observed in specialized systems, could be responsible for the increased versatility at the expense of a high catalytic activity. A comparison of DHP A and B, along with the systematic investigation of the amino acid differences between the two, provides a perfect system to elucidate in detail structure-function relationships of multifunctional systems to achieve the complexity required for increased activity of monofunctional systems.

The protein structure-function relationships of DHP were probed using 21 mutants of DHP A. Activity assays (peroxidase and peroxygenase) and binding studies elucidated the I9L mutation to be a key determinant in the structure-function relationships between isoenzymes A and B. The I9L containing mutants exhibited similar binding affinities of 5-Br-indole and 5-I-indole, as DHP B. In addition, the I9L mutant showed a synergistically beneficial effect with other single and double mutants. These findings were unexpected due to the location of the I9L mutation in relation to distal pocket. Position 9 is located in a hydrophobic region of the enzyme and does not have a direct contact with heme pocket. However, it may have an effect on the pocket through steric interactions with adjacent amino acid residues.

Examination of the Q-bands in the UV-vis spectra of the DHP A mutants presented an interesting competing effect involving the I9L, Y34N and S91G mutations. The addition of

the Y34N substitution increases the observed population of the oxyferrous form of the enzyme, which was confirmed by resonance Raman spectroscopy. However, the addition of the I9L substitution to Y34N containing mutants results in a minor increase in the five-coordinate ferric heme population and a subsequent decrease of the oxyferrous form of the enzyme. Furthermore, the addition of the S91G substitution to the Y34N containing mutants is able to virtually reverse the effect of Y34N mutation and prevent the increased reduction of the ferric enzyme to oxyferrous form.

© Copyright 2015 Roman Gavenko

All Rights Reserved

Investigating the Effects of Structural Changes to Enzymatic Activity in Isoenzymes of
Dehaloperoxidase from *Amphitrite ornata*

by
Roman Gavenko

A thesis submitted to the Graduate Faculty of
North Carolina State University
in partial fulfillment of the
requirements for the degree of
Master of Science

Chemistry

Raleigh, North Carolina

2015

APPROVED BY:

Stefan Franzen

Gavin J. Williams

Reza A. Ghiladi
Committee Chair

BIOGRAPHY

Roman Gavenko was born in Alushta (USSR) on May 7th in 1982. In 1995, he and his family settled in Bloomfield, New Jersey. He graduated from Bloomfield High School in 2000 and joined the workforce. In 2012, he graduated from William Paterson University in New Jersey with a Bachelor of Science in Chemistry and relocated to North Carolina to pursue graduate studies in chemistry. Roman continued his educational endeavors by joining the Department of Chemistry at North Carolina State University, where he conducted research under the direction of Dr. Reza Ghiladi.

ACKNOWLEDGMENTS

I would like to thank Dr. Reza Ghiladi and the members of my committee for their support and guidance throughout my studies and research with the Department of Chemistry at North Carolina State University. I would also like to extend my appreciation to all members of the Ghiladi group for engaging in many interesting discussions and for making my days in the lab more fun. Lastly, I would like to thank my family and friends for their continuous encouragement and support.

TABLE OF CONTENTS

LIST OF TABLES	vi
LIST OF FIGURES	vii
Chapter 1 – General Introduction	1
Dehaloperoxidase from <i>Amphitrite ornata</i> : General Properties	1
Comparison of Structural and Mechanistic Features of DHP, Peroxidases, and Globins	3
Peroxidase and Peroxygenase Activity of DHP	11
Investigation of Structure-Function Relationships of DHP	13
References	15
Chapter 2 – Spectroscopic Features and Enzymatic Activity of DHP Mutants	19
Introduction	19
Experimental	20
<i>Materials</i>	20
<i>Construction of Mutant DHP Plasmids</i>	21
<i>Protein Expression and Purification</i>	21
<i>Molecular Weight Determination</i>	23
<i>Preparation of Ferric DHP</i>	24
<i>Peroxidase Studies</i>	25
<i>Peroxygenase Studies</i>	25
<i>Stopped-Flow UV-visible Studies</i>	26
<i>5-Br-indole Binding Studies</i>	26
<i>Resonance Raman Studies</i>	26
Results and Discussion	27
<i>UV-Visible Spectra of the Mutants in the Resting (Fe^{3+} Heme) State</i>	27
<i>Peroxidase Studies</i>	41
<i>Peroxygenase Studies</i>	44
<i>Stopped-Flow UV-visible Studies</i>	46
<i>5-Br-indole Binding Studies</i>	50
<i>Resonance Raman Studies</i>	51
Conclusions	54

References	56
------------------	----

LIST OF TABLES

Table 2.1	Mutagenic Primers Used to Construct the DHP A Mutants.....	21
Table 2.2	Calculated monomeric molecular weights and experimentally determined weights of the dehaloperoxidase mutants.....	24
Table 2.3	UV-visible spectroscopic features of the DHP A variants and DHP B in the ferric heme state at pH 7.....	35
Table 2.4	UV-visible spectroscopic features and estimated oxyferrous form of the DHP A variants and DHP B over 360 hours at pH 7.....	41
Table 2.5	Kinetic Data for the Oxidative Catalytic Reaction of TCP with DHP enzymes.....	43
Table 2.6	Enzyme-Catalyzed Reactivity of 5-Br-Indole with DHP Mutants.....	46
Table 2.7	UV-visible spectroscopic features and rate of formation of Compound ES in DHP A and DHP B variants obtained with single mix stopped-flow experiment at pH 7.....	50
Table 2.8	UV-visible spectroscopic features and rate of formation of Compound RH in DHP A and DHP B variants obtained with single mix stopped-flow experiment at pH 7.....	50
Table 2.9	Dissociation Constants for 5-Br-indole and 5-I-indole.....	51

LIST OF FIGURES

Figure 1.1	Marine terebellid polychaete <i>Amphitrite ornata</i>	2
Figure 1.2	(A) DHP A WT (PDB: 4DWU). (B) DHP B WT (PDB: 3IXF).....	2
Figure 1.3	Clockwise (top left): DHP A (PDB: 2QFK), SWMB (PDB: 1A6K), HRP (PDB: 1W4Y), CcP (PDB: 1ZBY).....	4
Figure 1.4	Protoporphyrin IX (Heme B).....	5
Figure 1.5	Oxidation states of the heme group. AA represents an amino acid from the surrounding protein.....	6
Figure 1.6	The classic peroxidase cycle with hydrogen peroxide and phenol.....	7
Figure 1.7	General representation of Poulos-Kraut “push-pull” effect in peroxidases.....	9
Figure 1.8	Open and closed conformations of the distal histidine in DHP B (PDB: 3IXF).....	10
Figure 1.9	Active sites of (A) DHP A (PDB: 2QFK) and (B) HRP (PDB: 1W4).....	11
Figure 1.10	Peroxidase Reaction of Trihalophenol Oxidative Dehalogenation by DHP....	12
Figure 1.11	Peroxygenase Reaction for the Oxidation of Indole by DHP.....	13
Figure 2.1	Dehaloperoxidase A (DHP A) (PDB: 4DWU). The heme group, the proximal and distal histidines (His89 and His55, respectively), and 5 amino acids that differ in DHP B are highlighted.....	20
Figure 2.2	The UV-visible spectra of WT DHP A, WT DHP B, DHP A (I9L), DHP B (L9I) and DHP A (I9V) at pH 7.....	31
Figure 2.3	The UV-visible spectra of DHP A (R32K), DHP A (Y34N), DHP A (N81S) and DHP A (S91G) at pH 7.....	32
Figure 2.4	The UV-visible spectra of DHP A (I9L/R32K), DHP A (I9L/Y34N), DHP A (I9L/N81S) and DHP A (I9L/S91G) at pH 7.....	32
Figure 2.5	The UV-visible spectra of DHP A (R32K/Y34N), DHP A (R32K/N81S), DHP A (R32K/S91G), DHP A (Y34N/N81S), DHP A (Y34N/S91G) and DHP A (N81S/S91G) at pH 7.....	33

Figure 2.6	The UV-visible spectra of DHP A (I9L/R32K/Y34N), DHP A (I9L/R32K/N81S), DHP A (I9L/R32K/S91G), DHP A (I9L/Y34N/N81S), DHP A (I9L/Y34N/S91G) and DHP A (I9L/N81S/S91G) at pH 7.....	33
Figure 2.7	The UV-visible spectra of DHP A (Y34N), DHP A (I9L/Y34N), DHP A (R32K/Y34N), DHP A (Y34N/N81S), DHP A (Y34N/S91G), DHP A (I9L/R32K/Y34N), DHP A (I9L/Y34N/N81S) and DHP A (I9L/Y34N/S91G) at pH 7.....	34
Figure 2.8	Scatter plot of A_{Soret}/A_{380} vs A_{614}/A_{645} of DHP enzymes listed in Table 2.3....	34
Figure 2.9	The UV-visible spectra of WT DHP A in aerobic conditions over 360 hours at pH 7.....	36
Figure 2.10	The UV-visible spectra of WT DHP B in aerobic conditions over 360 hours at pH 7.....	36
Figure 2.11	The UV-visible spectra of DHP A (I9L) in aerobic conditions over 360 hours at pH 7.....	37
Figure 2.12	The UV-visible spectra of DHP A (Y34N) in aerobic conditions over 360 hours at pH 7.....	37
Figure 2.13	The UV-visible spectra of DHP A (S91G) in aerobic conditions over 360 hours at pH 7.....	38
Figure 2.14	The UV-visible spectra of DHP A (I9L/Y34N) in aerobic conditions over 360 hours at pH 7.....	38
Figure 2.15	The UV-visible spectra of DHP A (I9L/S91G) in aerobic conditions over 360 hours at pH 7.....	39
Figure 2.16	The UV-visible spectra of DHP A (Y34N/S91G) in aerobic conditions over 360 hours at pH 7.....	39
Figure 2.17	The UV-visible spectra of DHP A (I9L/Y34N/S91G) in aerobic conditions over 360 hours at pH 7.....	40
Figure 2.18	The UV-visible spectra of DHP B (L9I) in aerobic conditions over 360 hours at pH 7.....	40

Figure 2.19	Ile9 and adjacent residues in WT DHP A (PDB: 4DWU).....	44
Figure 2.20	Reference stopped-flow UV-visible spectra of DHP A (I9L/Y34N/S91G) (10 μ M) reacting with 10-fold excess of H ₂ O ₂ at pH 7 (900 scans over 83 s); <i>inset</i> , the single wavelength (419 nm) dependence of time obtained from the raw spectra and its fit with a superposition of the calculated spectra components.....	49
Figure 2.21	Reference calculated spectra of the three reaction components derived from the SVD analysis of data from Figure 2.20: ferric heme state (black), Compound ES (red) and Compound RH (blue).....	49
Figure 2.22	Reference time dependences of the relative concentrations for the three components as shown in the Figure 2.21 determined by fitting the spectra set in Figure 2.20.....	48
Figure 2.23	Resonance Raman spectra of DHP A (I9L) (solid line), WT DHP A (dashed line), WT DHP B (dotted line) in 100 mM KP _i (black), in 10% MeOH/100 mM KP _i (v/v) (red), 1 mM 5-Br-indole (green) and 5-I-indole (blue) in 10% MeOH/100 mM KP _i (v/v) at pH 7.....	53
Figure 2.24	Resonance Raman spectra of DHP A (I9L/Y34N) (solid line), WT DHP A (dashed line), WT DHP B (dotted line) in 100 mM KP _i (black), in 10% MeOH/100 mM KP _i (v/v) (red), 1 mM 5-Br-indole (green) and 5-I-indole (blue) in 10% MeOH/100 mM KP _i (v/v) at pH 7.....	54

Chapter 1

General Introduction

Dehaloperoxidase from *Amphitrite ornata*: General Properties

A variety of infaunal marine annelids, such as *Notomastus lobatus*, *Saccoglossus kowalevskii*, and *Thelepus crispus*, secrete high levels of halogenated secondary metabolites, such as mono-, di-, and tribromophenols^{1,2} and brominated indoles^{3,4}, as means of territorial protections.⁵⁻⁷ *Amphitrite ornata* (Figure 1.1), a terebellid polychaete, is able to co-inhabit in the same environment due to its ability to perform, in part, the H₂O₂-dependent oxidative dehalogenation of toxic mono-, di-, and trisubstituted halophenols that possess bromine, chlorine and fluorine substituents with dehalogenating enzymes, such as dehaloperoxidase (DHP).^{5, 6, 8} DHP, the most abundant protein in the organism, is a coelomic enzyme that is capable of reversible oxygen binding^{9, 10}, peroxidase activity^{8, 11-21} and recently reported peroxygenase and oxidase activities²². Two isoenzymes of DHP, A and B, have been isolated and characterized; both are encoded by separate genes that presumably arisen from a gene duplication and are not alleles of a single gene.⁵ DHP B differs from DHP A by 5 amino acids (I9L, R32K, Y34N, N81S, and S91G) (Figure 1.2), but exhibits improved peroxidase and peroxygenase activities.^{12, 22, 23} However, the primary functions of DHP are oxygen storage and transport protein, as suggest by Dr. Joseph Bonaventura when DHP was first identified as the coelomic hemoglobin of *A. ornata*.^{9, 24-26} In line with this suggestion, DHP is isolated in an oxyferrous state without presence of any reductant during purification. In contrast, most heme-containing proteins, particularly peroxidases, are isolated in ferric state.²⁰ In addition, this result has been confirmed by formation of carbonmonoxy ferrous derivative in the presence of carbon monoxide, a ligand which only binds to the ferrous oxidation state of heme proteins.²⁷ It has been proposed that the DHP enzymatic functions have evolved from an oxygen carrying globin through gene duplication and divergence due to environmental pressures^{28, 29}, while conserving proximal and distal histidine residues as observed in globins and Type III peroxidases.^{17, 27} Also, the optimum activity of Type III peroxidases is at pH <5.5, but the optimal catalytic activity of DHP is achieved at the physiological pH of 7.4.³⁰ However, in

light of newly discovered capabilities of DHP, it has been proposed that DHP represents a multifunctional “template” enzyme with a limited protein scaffolding, and may be an ancestor to more specialized, high catalytic activity enzymes.²²

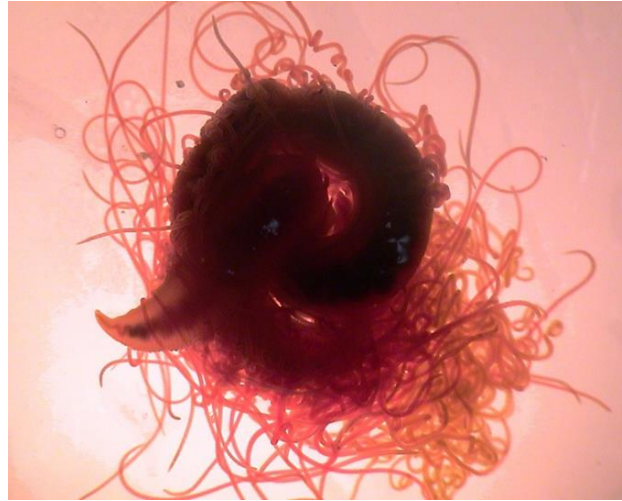


Figure 1.1. Marine terebellid polychaete *Amphitrite ornata*.

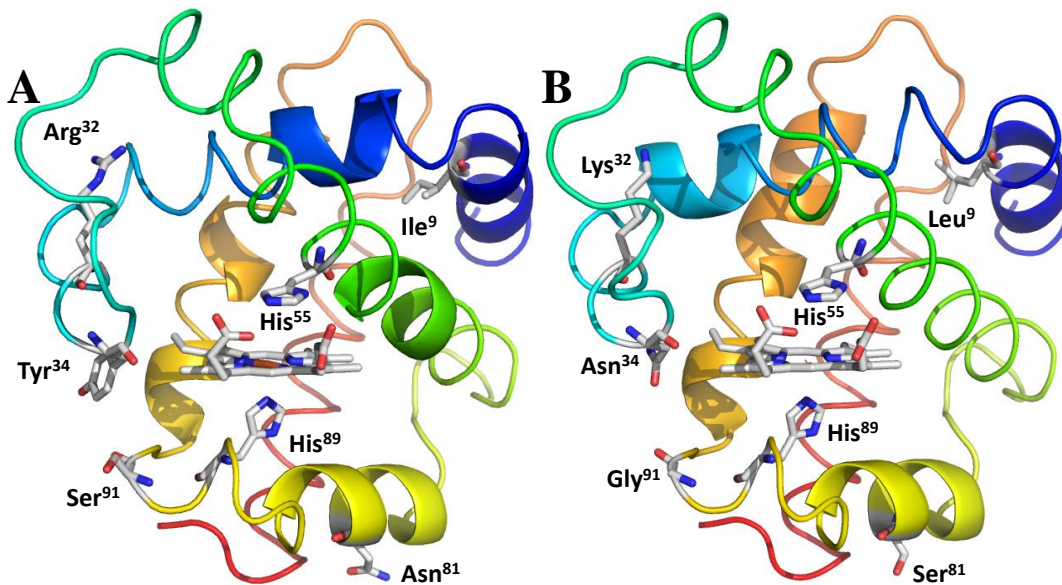


Figure 1.2. (A) DHP A WT (PDB: 4DWU). (B) DHP B WT (PDB: 3IXF).

Comparison of Structural and Mechanistic Features of DHP, Peroxidases, and Globins

The X-ray crystal structures showed that DHP has a characteristic globin fold composed of the canonical 3/3 α -helical structure, and has been characterized by the Structural Classification of Proteins (SCOP) as a globin.^{7, 28, 31, 32} However, DHP has very little sequence homology compared to other myoglobins (Mbs) and hemoglobins (Hbs).²³ Even though DHP is capable of peroxidase activity, it shows little similarity to the fold of other well characterized peroxidases such as cytochrome *c* peroxidase (CcP) and horseradish peroxidase (HRP) (Figure 1.3).³³

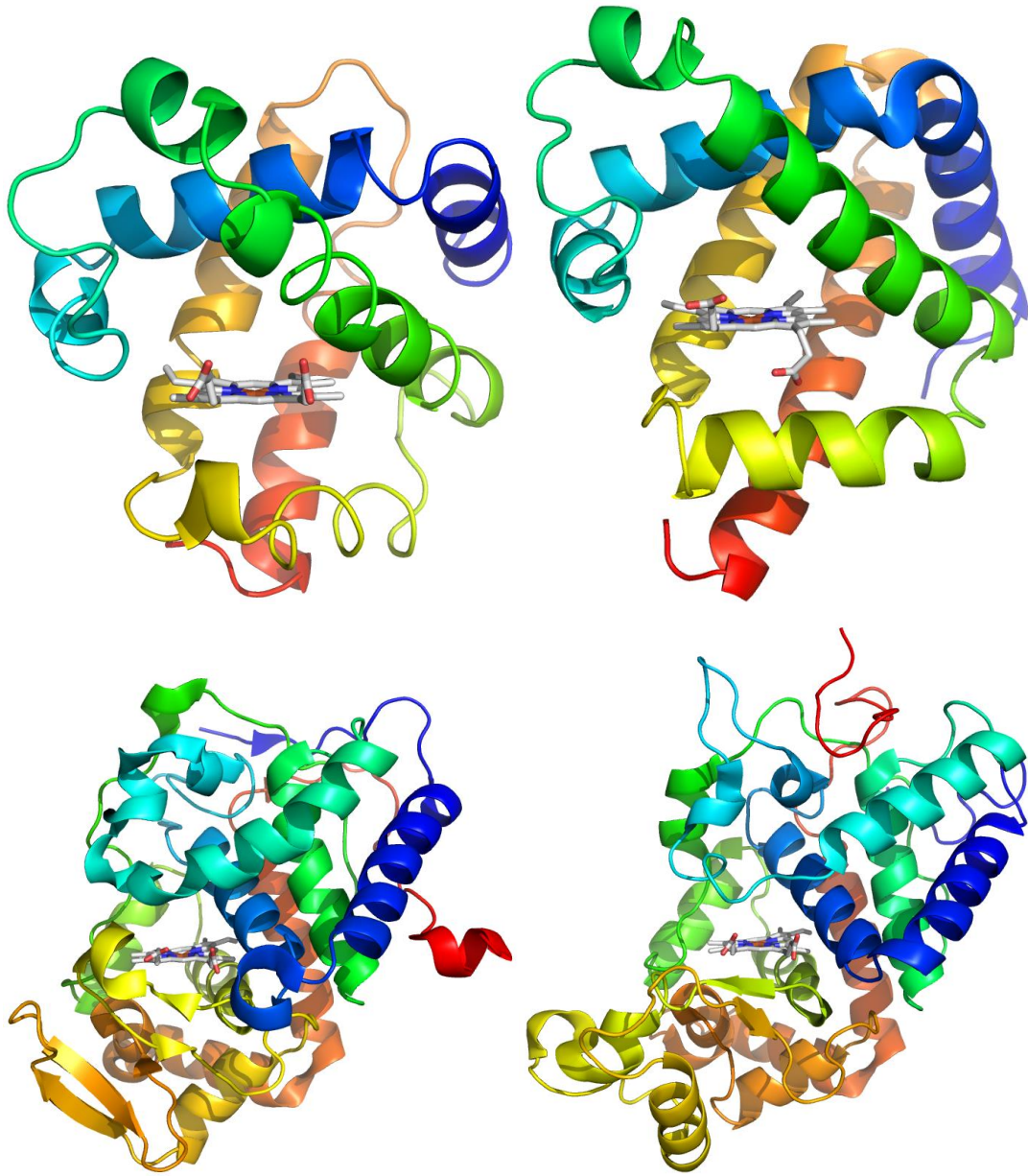


Figure 1.3. Clockwise (top left): DHP A (PDB: 2QFK), SWMB (PDB: 1A6K), HRP (PDB: 1W4Y), CcP (PDB: 1ZBY).

Globins and the majority of peroxidases contain protoporphyrin IX (Heme B), a prosthetic group containing an iron atom complexed to four equatorial-positioned nitrogen atoms from the pyrrole groups of a porphyrin macrocycle (Figure 1.4). DHP and globins have

an evolutionary-conserved fifth ligand, a histidine residue (proximal histidine) that holds protoporphyrin IX to the surrounding protein matrix (apoprotein) with a single coordination bond to the iron. In nitric oxide synthase (NOS) and cytochrome P450 (P450), a proximal cysteine residue occupies this position instead of the proximal histidine. A crucial histidine ligand is located on the distal side of the heme, and it is essential in hydrogen bond stabilization of the sixth exogenous ligand such as dioxygen, water, and peroxide molecules. In order for catalytic activity to occur, the heme group must be able to shuttle between various oxidation states (Figure 1.5).

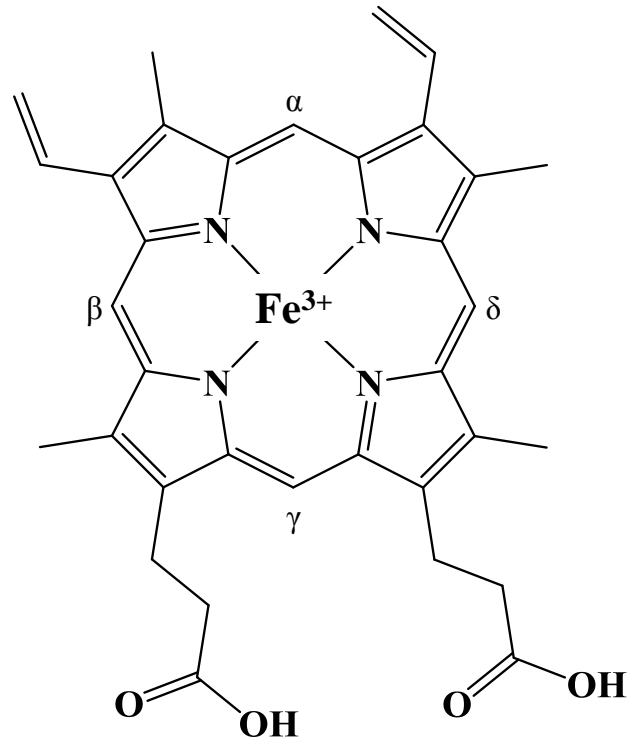


Figure 1.4. Protoporphyrin IX (Heme B).

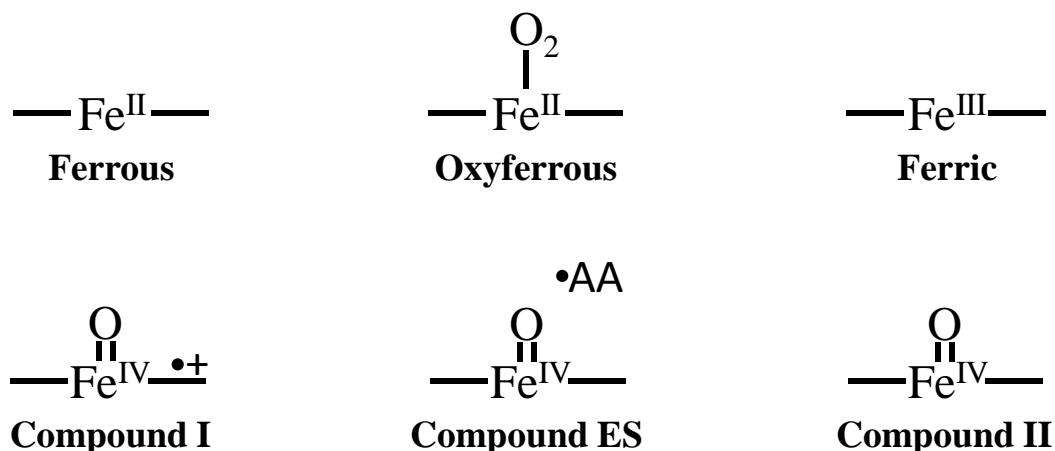


Figure 1.5. Oxidation states of the heme group. AA represents an amino acid from the surrounding protein.

The first description of a general mechanism of heme peroxidases was published by Poulos *et al.* in 1980 (Figure 1.6).³³ The classic peroxidase cycle arises from a resting ferric form of the enzyme. The first step involves the formation ferric hydroperoxide Fe-OOH (Compound 0) by deprotonation of the hydrogen molecule by distal histidine and subsequent displacement of a heme-bound water molecule (step i). A water molecule is evolved upon heterolytic O-O bond cleavage to form Compound I, a ferryl iron center with a π -cation radical on the porphyrin macrocycle, after a two electron oxidation of Heme B (step iii). Compound I performs a one electron reduction with the substrate (PhOH) to form Compound II, a ferryl species (step iii). In the final step, the resting ferric form of the enzyme is restored by a one electron reduction of Compound II with the substrate (step iv).

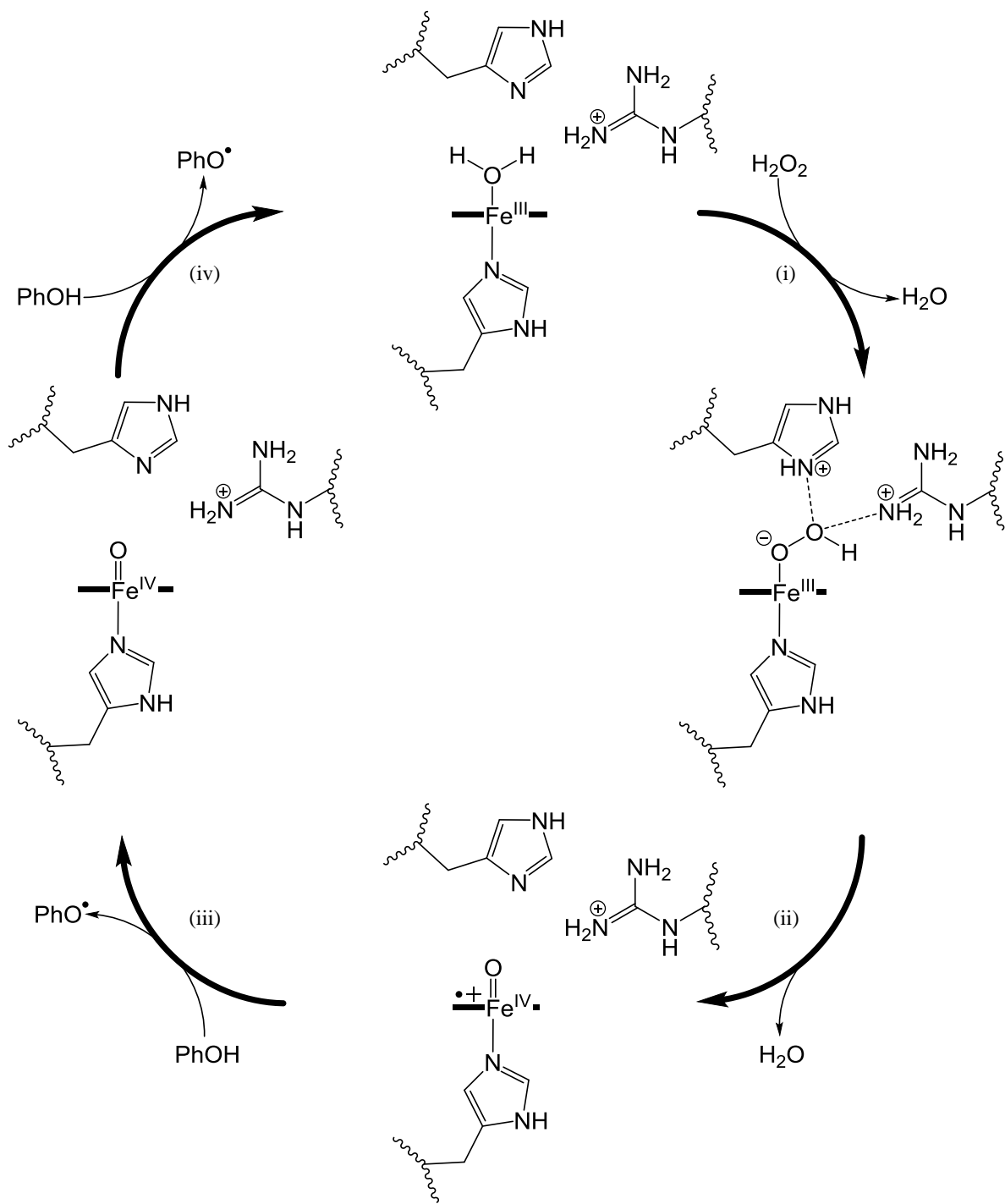


Figure 1.6. The classic peroxidase cycle with hydrogen peroxide and phenol.

DHP represents a true multifunctional enzyme containing features of both globins and peroxidases. Globins and DHP possess a distal pocket that is essentially entirely hydrophobic. In globins, the hydrophobic nature of the distal pocket minimizes the chances of undesired chemistry with the bound substrates, such as dioxygen and carbon dioxide. However, in DHP the distal pocket is well suited to help to stabilize the internal binding of monohalogenated phenols.^{34, 35} In contrast, in HRP and CcP, the distal cavities contain an arginine residue that polarizes the O-O bond by stabilization of the developing negative charge on the oxygen atom of the peroxide molecule during heterolytic cleavage in the “pull effect” of the Poulos-Kraut mechanism (Figure 1.7).^{33, 36, 37} Since peroxidases perform the reactions at the heme edge the charged residue in the distal pocket does not have an effect on the substrate binding.

The evolutionary-conserved proximal histidine ligand is involved in heterolytic O-O bond cleavage necessary for Compound I formation.³⁶ In HRP, a negatively charged carboxylate sidechain from an aspartic acid is located within 2.8 Å (PDB: 1W4Y) of the proximal histidine and creates a strong H-bond interaction with the imidazole N_δH of the proximal histidine (Figure 1.9B).³⁷ This interaction results in the imidazole N_ε of the proximal histidine to obtain an anionic character, which is crucial for the stabilization of the high-oxidation states of the heme iron in Compounds I and II and is known as the Asp-His-Fe catalytic triad.^{33, 37} The increase in electron density on the heme assists in the heterolytic cleavage of the O-O bond of the hydrogen peroxide molecule and has been identified as the “push” effect, which works in tandem with the “pull” effect in the Poulos-Kraut “push-pull” mechanism (Figure 1.7). In recent studies of cytochrome *c* peroxidase, mutants indicated that the “push” effect plays a minor role in catalytic activity when compared to the “pull” effect.^{28,}

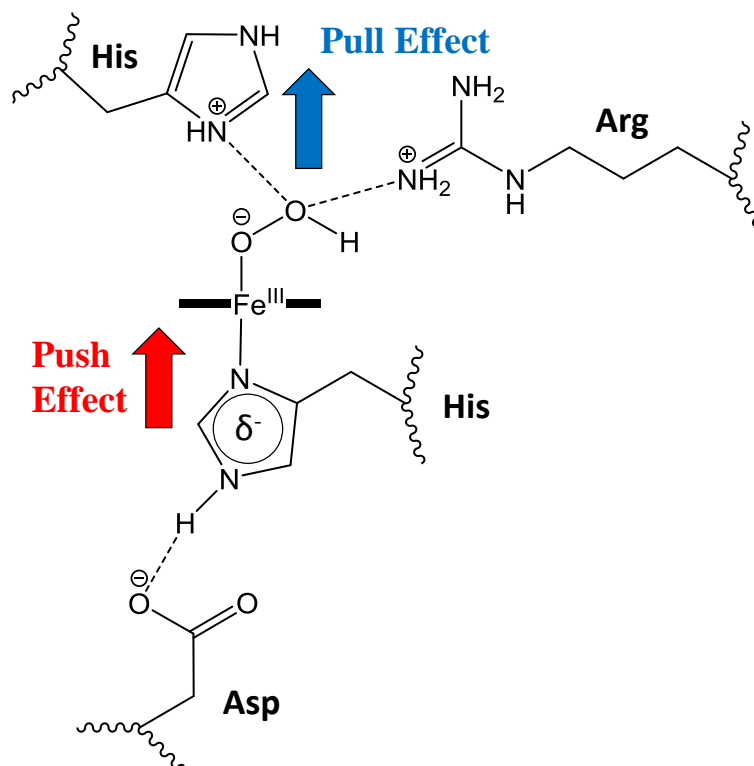


Figure 1.7. General representation of Poulos-Kraut “push-pull” effect in peroxidases.

Similar to globins, DHP contains a distal histidine, which has been observed in two different conformations: solvent exposed (open) and internal (closed) conformations (Figure 1.8). In the closed conformation, the distal histidine is able to stabilize heme-bound water or dioxygen molecules through hydrogen bonding.³¹ Structural analysis of DHP established that the distance from the heme iron to the N_δH of the distal histidine is 5.4 Å, and its heme moiety is located 1.5 Å deeper in the protein compared to Mb.^{28, 31} In globins and peroxidases, the distances have been reported as 4.1 to 4.6 Å and 5.5 to 6.0 Å, respectively.²⁸ This shift allows for increased flexibility of the distal histidine to make it more peroxidase-like, and is possible due to a substitution of a glycine residue in Mb by a threonine residue in DHP located after the distal histidine in the primary amino acid sequence.^{14, 31, 39}

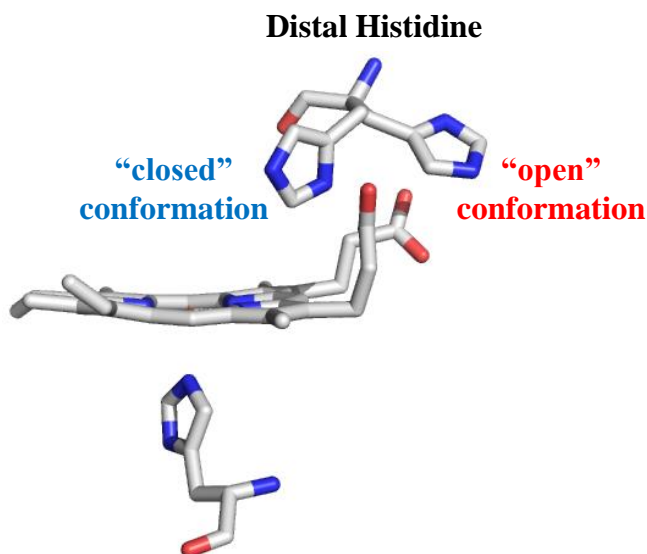


Figure 1.8. Open and closed conformations of the distal histidine in DHP B (PDB: 3IXF).

However, DHP does not have an aspartic acid residue and resembles more of a globin configuration with a slight variation (Figure 1.9A). The imidazole ring of the proximal histidine is rotated by $\sim 60^\circ$ with the respect to the position in globins. This rotation aligns the imidazole N_δH with the oxygen atom of the leucine peptide carbonyl, resulting in a stronger bond than in Mb. This reorientation is due to a shift of the proximal histidine by two residues towards the N-terminus end, and replacement of the last turn of the α -helix with a short 3₁₀ helix, compared to Mb.²⁸ Even with the improved hydrogen bonding, the imidazole of the proximal histidine maintains a mostly neutral character.^{14, 21, 37}

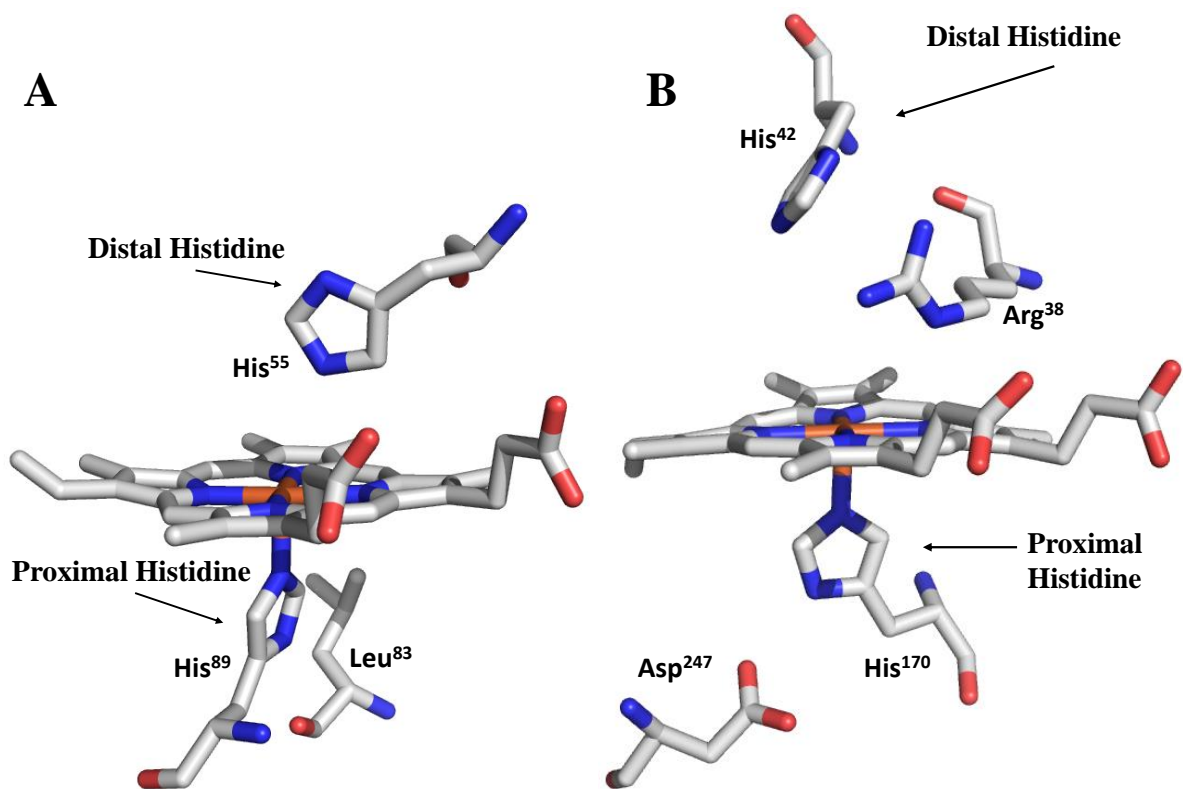


Figure 1.9. Active sites of (A) DHP A (PDB: 2QFK) and (B) HRP (PDB: 1W4Y).

Peroxidase and Peroxygenase Activity of DHP

DHP possesses the capability to perform the H_2O_2 -dependent oxidative dehalogenation of various toxic haloaromatic compounds such as trihalogenated phenols (Figure 1.10).⁶ Studies have shown that DHP A oxidizes 2,4,6-TBP to 2,6-DCQ at rates approximately tenfold faster than myoglobin but tenfold slower than HRP¹⁰, and DHP B is about 3 times faster than DHP A.¹² DHP reacts with hydrogen peroxide to generate Compound I, which converts to Compound ES through internal electron transfer.¹¹ The overall two-electron cosubstrate oxidation proceeds through discrete one-electron steps, similar to other peroxidases.¹⁸ However, the uniqueness of DHP is its ability to initiate the catalytic cycle from oxy-/ferrous state, and to be able to return to the globin active state after the peroxidase cycle is complete. This return is possible due to an extremely high redox potential of +204 and +206 mV for DHP

A and DHP B, respectively.⁴⁰ In comparison to other myoglobins and hemoglobins, DHP has a significantly more stable ferrous form with the exception of the giant extracellular hemoglobin from *Lumbricus*.²³

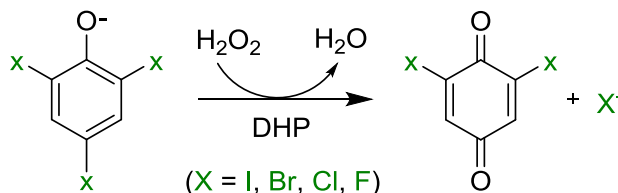


Figure 1.10. Peroxidase Reaction of Trihalophenol Oxidative Dehalogenation by DHP.

Another unique feature of DHP is the formation of Compound RH from Compound ES in the absence of trihalophenol cosubstrate.^{11, 12, 20, 23} It has been hypothesized that this inactivation of DHP occurs due to protein-heme crosslink¹³, but this has yet to be fully elucidated. It is suggested that the Compound RH form may protect the organism from deleterious oxidation chemistry by shifting DHP to a less active form.^{11, 23}

In a recent work²², the ability of DHP to catalyze the oxidation of brominated indoles using H_2O_2 as the oxidizing agent has been investigated. The results obtained with labeled peroxide confirmed a previously unreported peroxygenase activity similar to the peroxide shunt pathway of P450 monooxygenase (Figure 1.11).^{22, 41, 42} Similar to the peroxidase reaction, the peroxygenase activity could be initiated from either the ferric or oxyferrous states. Also, the enzyme was able to return to oxyferrous state upon completion of its activity due to a unique product-driven oxidase reaction that forms indigo derivatives as products.²²

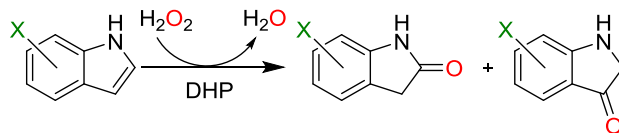


Figure 1.11. Peroxygenase Reaction for the Oxidation of Indole by DHP.

The peroxygenase reaction is a one-step incorporation of the oxygen atom from Compound I/ES into product, which itself was acquired during the heterolytic cleavage of hydrogen peroxide. This reaction requires that the haloindole substrate be within close distance of the heme center. Resonance Raman studies showed that presence of 5-Br-indole perturbs the relative population of 5-coordinated high spin (5cHS) vs. 6-coordinated high spin (6cHS) ferric hemes, similar to 4-halophenol.^{22, 43} A known inhibitor of DHP, 4-halophenol, binds inside the distal cavity and disrupts the hydrogen bonding between iron-bound water and distal histidine by displacing the distal histidine into an “open” conformation, with the magnitude of the shift correlating to the size of the halogen atom.^{43, 44} It has been hypothesized that 5-Br-indole binds in the monohalophenol inhibitor site, which is right above the heme iron. In addition, a 7-Br-indole can be accommodated in the trihalophenol binding site by the α -edge of the heme, while the heme iron is in 6cHS state.

Investigation of Structure-Function Relationships of DHP

Two isoenzymes of DHP, A and B, are encoded by separate genes and are not alleles of a single gene.⁵ DHP B differs from DHP A by 5 amino acids (I9L, R32K, Y34N, N81S, and S91G) and exhibits a threefold increase in peroxidase activity compared to DHP A.^{12, 22, 23} Also, the amino acid substitutions in DHP B modify the radical pathway involved in formation of Compound ES.¹⁶ Uniquely to DHP, both of the enzymes form Compound RH in the absence of a trihalophenol cosubstrate, but UV-visible spectroscopic properties are different in DHP B¹² compared to DHP A¹¹. Despite the differences introduced by the mutation of five amino acids, both enzymes have nearly identical formal reduction potentials of 202 ± 6 mV⁴⁰ and 206 ± 6 mV¹² for DHP A and DHP B, respectively. DHP represents a truly unique enzyme due to

its ability to perform a diverse range of functions. The flexibility of this heme enzyme comes at a cost of decreased catalytic activity and efficiency compared to specialized monofunctional counterparts. The unique nature of the DHP active site, which lacks the additional structural features observed in specialized systems, could be responsible for the increased versatility at the expense of a high catalytic activity. A comparison of DHP A and B, along with the systematic investigation of the amino acid differences between the two, provides a perfect system to elucidate in detail structure-function relationships of multifunctional systems to achieve the complexity required for increased activity of monofunctional systems.

References:

1. Woodin, S. A.; Walla, M. D.; Lincoln, D. E. Occurrence of brominated compounds in soft-bottom benthic organisms. *J. Exp. Mar. Biol. Ecol.* **1987**, *107*, 209-217.
2. Woodin, S. A. Recruitment of Infauna: Positive or Negative Cues? *Amer. Zool.* **1991**, *31* (6), 797-807.
3. Gribble, G. W. The diversity of naturally occurring organobromine compounds. *Chem. Soc. Rev.* **1999**, *28*, 335-346.
4. Gribble, G. W. The natural production of organobromine compounds. *Environ. Sci. Pollut. Res. Int.* **2000**, *7* (1), 37-49.
5. Han, K.; Woodin, S. A.; Lincoln, D. E.; Fielman, K. T.; Ely, B. Amphitrite ornata, a marine worm, contains two dehaloperoxidase genes. *Mar Biotechnol (NY)* **2001**, *3* (3), 287-92.
6. Chen, Y. P.; Woodin, S. A.; Lincoln, D. E.; Lovell, C. R. An Unusual Dehalogenating Peroxidase from the Marine Terebellid Polychaete *Amphitrite ornata*. *J. Biol. Chem.* **1996**, *271* (9), 4609-4612.
7. Lebioda, L.; LaCount, M. W.; Zhang, E.; Chen, Y. P.; Han, K.; Whitton, M. M.; Lincoln, D. E.; Woodin, S. A. An enzymatic globin from a marine worm. *Nature* **1999**, *401*, 445.
8. Osborne, R. L.; Taylor, L. O.; Han, K. P.; Ely, B.; Dawson, J. H. Amphitrite ornata dehaloperoxidase: enhanced activity for the catalytically active globin using MCPBA. *Biochem Biophys Res Commun* **2004**, *324* (4), 1194-8.
9. Weber, R. E.; Mangum, C.; Steinman, H.; Bonaventura, C.; Sullivan, B.; Bonaventura, J. Hemoglobins of two terebellid polychaetes: *Enoplobranchus sanguineus* and *Amphitrite ornata*. *Comp. Biochem. Physiol.* **1977**, *56A*, 179-187.
10. Belyea, J. L.; Gilvey, L. B.; Davis, M. F.; Godek, M.; Sit, T. L.; Lommel, S. A.; Franzen, S. Enzyme Function of the Globin Dehaloperoxidase from *Amphitrite ornata* Is Activated by Substrate Binding. *Biochemistry* **2005**, *44* (48), 15637-15644.
11. Feducia, J.; Dumarieh, R.; Gilvey, L. B.; Smirnova, T.; Franzen, S.; Ghiladi, R. A. Characterization of dehaloperoxidase compound ES and its reactivity with trihalophenols. *Biochemistry* **2009**, *48* (5), 995-1005.
12. D'Antonio, J.; D'Antonio, E. L.; Thompson, M. K.; Bowden, E. F.; Franzen, S.; Smirnova, T.; Ghiladi, R. A. Spectroscopic and Mechanistic Investigations of Dehaloperoxidase B from *Amphitrite ornata*. *Biochemistry* **2010**, *49* (31), 6600-16.

13. Thompson, M.; Franzen, S.; Ghiladi, R. A.; Reeder, B. J.; Svistunenko, D. A. Compound ES of Dehaloperoxidase Decays via Two Alternative Pathways Depending on the Conformation of the Distal Histidine. *J Am Chem Soc* **2010**, *132* (49), 17501-17510.
14. D'Antonio, E. L.; D'Antonio, J.; de Serrano, V.; Gracz, H.; Thompson, M. K.; Ghiladi, R. A.; Bowden, E. F.; Franzen, S. Functional consequences of the creation of an Asp-His-Fe triad in a 3/3 globin. *Biochemistry* **2011**, *50* (44), 9664-80.
15. D'Antonio, J.; Ghiladi, R. A. Reactivity of deoxy- and oxyferrous dehaloperoxidase B from *Amphitrite ornata*: identification of compound II and its ferrous-hydroperoxide precursor. *Biochemistry* **2011**, *50* (27), 5999-6011.
16. Dumarieh, R.; D'Antonio, J.; Deliz-Liang, A.; Smirnova, T.; Svistunenko, D. A.; Ghiladi, R. A. Tyrosyl radicals in dehaloperoxidase: how nature deals with evolving an oxygen-binding globin to a biologically relevant peroxidase. *J Biol Chem* **2013**, *288* (46), 33470-82.
17. Osborne, R. L.; Sumithran, S.; Coggins, M. K.; Chen, Y. P.; Lincoln, D. E.; Dawson, J. H. Spectroscopic characterization of the ferric states of *Amphitrite ornata* dehaloperoxidase and *Notomastus lobatus* chloroperoxidase: His-ligated peroxidases with globin-like proximal and distal properties. *J Inorg Biochem* **2006**, *100* (5-6), 1100-8.
18. Osborne, R. L.; Coggins, M. K.; Raner, G. M.; Walla, M.; Dawson, J. H. The mechanism of oxidative halophenol dehalogenation by *Amphitrite ornata* dehaloperoxidase is initiated by H₂O₂ binding and involves two consecutive one-electron steps: role of ferryl intermediates. *Biochemistry* **2009**, *48* (20), 4231-8.
19. Davydov, R.; Osborne, R. L.; Shanmugam, M.; Du, J.; Dawson, J. H.; Hoffman, B. M. Probing the Oxyferrous and Catalytically Active Ferryl States of *Amphitrite ornata* Dehaloperoxidase by Cryoreduction and EPR/ENDOR Spectroscopy. Detection of Compound I. *J Am Chem Soc* **2010**, *132* (42), 14995-15004.
20. Du, J.; Sono, M.; Dawson, J. H. Functional switching of *Amphitrite ornata* dehaloperoxidase from O₂-binding globin to peroxidase enzyme facilitated by halophenol substrate and H₂O₂. *Biochemistry* **2010**, *49* (29), 6064-9.
21. de Serrano, V.; D'Antonio, J.; Franzen, S.; Ghiladi, R. A. Structure of dehaloperoxidase B at 1.58 Å resolution and structural characterization of the AB dimer from *Amphitrite ornata*. *Acta Crystallogr D Biol Crystallogr* **2010**, *66* (Pt 5), 529-38.
22. Barrios, D. A.; D'Antonio, J.; McCombs, N. L.; Zhao, J.; Franzen, S.; Schmidt, A. C.; Sombers, L. A.; Ghiladi, R. A. Peroxygenase and Oxidase Activities of Dehaloperoxidase-Hemoglobin from *Amphitrite ornata*. *J Am Chem Soc* **2014**.

23. Franzen, S.; Thompson, M. K.; Ghiladi, R. A. The dehaloperoxidase paradox. *Biochim Biophys Acta* **2012**, *1824* (4), 578-88.
24. Mangum, C.; Woodin, B. R.; Bonaventura, C.; Sullivan, B.; Bonaventura, J. The role of coelomic and vascular hemoglobin in the annelid family terebellidae. *Comp. Biochem. Physiol.* **1975**, *51A*, 281-294.
25. Chiancone, E.; Brenowitz, M.; Ascoli, F.; Bonaventura, C.; Bonaventura, J. *Amphitrite ornata* erythrocyruorin. I. Structural properties and characterization of subunit interactions. *Biochim Biophys Acta* **1980**, *623*, 146-162.
26. Chiancone, E.; Ferruzzi, G.; Bonaventura, C.; Bonaventura, J. *Amphitrite ornata* erythrocyruorin II. Molecular controls of function. *Biochim Biophys Acta* **1981**, *670*, 84-92.
27. Roach, M. P.; P., C. Y.; Woodin, S. A.; Lincoln, D. E.; Dawson, J. H. Notomastus lobatus Chloroperoxidase and Amphitrite ornata Dehaloperoxidase Both Contain Histidine as Their Proximal Heme Iron Ligand. *Biochemistry* **1997**, *36* (8), 2197-2202.
28. LaCount, M. W.; Zhang, E.; Chen, Y. P.; Han, K.; Whitton, M. M.; Lincoln, D. E.; Woodin, S. A.; Lebioda, L. The crystal structure and amino acid sequence of dehaloperoxidase from Amphitrite ornata indicate common ancestry with globins. *J Biol Chem* **2000**, *275* (25), 18712-6.
29. Du, J.; Huang, X.; Sun, S.; Wang, C.; Lebioda, L.; Dawson, J. H. Amphitrite ornata dehaloperoxidase (DHP): investigations of structural factors that influence the mechanism of halophenol dehalogenation using "peroxidase-like" myoglobin mutants and "myoglobin-like" DHP mutants. *Biochemistry* **2011**, *50* (38), 8172-80.
30. Franzen, S.; Gilvey, L. B.; Belyea, J. L. The pH dependence of the activity of dehaloperoxidase from Amphitrite ornata. *Biochim Biophys Acta* **2007**, *1774* (1), 121-30.
31. de Serrano, V.; Chen, Z.; Davis, M. F.; Franzen, S. X-ray crystal structural analysis of the binding site in the ferric and oxyferrous forms of the recombinant heme dehaloperoxidase cloned from Amphitrite ornata. *Acta Crystallogr D Biol Crystallogr* **2007**, *63* (Pt 10), 1094-101.
32. Lo Conte, L.; Ailey, B.; Hubbard, T.; Brenner, S. E.; Murzin, A. G.; Chothia, C. SCOP: a Structural Classification of Proteins database. *Nuc. Ac. Res.* **2000**, *28* (1), 257-259.
33. Poulos, T. L.; Kraut, J. The Stereochemistry of Peroxidase Catalysis. *J. Biol. Chem.* **1980**, *255* (17), 8199-8205.

34. Plummer, A.; Thompson, M. K.; Franzen, S. Role of polarity of the distal pocket in the control of inhibitor binding in dehaloperoxidase-hemoglobin. *Biochemistry* **2013**, *52* (13), 2218-27.
35. Zhao, J.; de Serrano, V.; Dumariéh, R.; Thompson, M.; Ghiladi, R. A.; Franzen, S. The role of the distal histidine in H₂O₂ activation and heme protection in both peroxidase and globin functions. *J Phys Chem B* **2012**, *116* (40), 12065-77.
36. Poulos, T. L. Thirty years of heme peroxidase structural biology. *Arch Biochem Biophys* **2010**, *500* (1), 3-12.
37. Battistuzzi, G.; Bellei, M.; Bortolotti, C. A.; Sola, M. Redox properties of heme peroxidases. *Arch Biochem Biophys* **2010**, *500* (1), 21-36.
38. Matsui, T.; Ozaki, S. i.; Liang, E.; Phillips, G. N.; Watanabe, Y. Effects of the Location of Distal Histidine in the Reaction of Myoglobin with Hydrogen Peroxide. *J. Biol. Chem.* **1999**, *274* (5), 2838-2844.
39. Chen, Z.; de Serrano, V.; Betts, L.; Franzen, S. Distal histidine conformational flexibility in dehaloperoxidase from *Amphitrite ornata*. *Acta Crystallogr D Biol Crystallogr* **2009**, *65* (Pt 1), 34-40.
40. D'Antonio, E. L.; Bowden, E. F.; Franzen, S. Thin-layer spectroelectrochemistry of the Fe(III)/Fe(II) redox reaction of dehaloperoxidase-hemoglobin. *J. Electroanal. Chem.* **2012**, *668*, 37-43.
41. Sono, M.; Roach, M. P.; Coulter, E. D.; Dawson, J. H. Heme-Containing Oxygenases. *Chem. Rev.* **1996**, *96* (7), 2841-2887.
42. Meunier, B.; de Visser, S. P.; Shaik, S. Mechanism of Oxidation Reactions Catalyzed by Cytochrome P450 Enzymes. *Chem. Rev.* **2004**, *104* (9), 3947-3980.
43. Thompson, M. K.; Davis, M. F.; de Serrano, V.; Nicoletti, F. P.; Howes, B. D.; Smulevich, G.; Franzen, S. Internal binding of halogenated phenols in dehaloperoxidase-hemoglobin inhibits peroxidase function. *Biophys J* **2010**, *99* (5), 1586-95.
44. Nicoletti, F. P.; Thompson, M. K.; Howes, B. D.; Franzen, S.; Smulevich, G. New Insights into the Role of Distal Histidine Flexibility in Ligand Stabilization of Dehaloperoxidase-Hemoglobin from *Amphitrite ornata*. *Biochemistry* **2010**, *49* (9), 1903-1912.

Chapter 2

Spectroscopic Features and Enzymatic Activity of DHP Mutants

Introduction

Dehaloperoxidase (DHP) from the terebellid polychaete *Amphitrite ornata* is the first oxygen-binding globin that possesses both biologically relevant peroxidase^{11, 16, 23} and peroxygenase²² activities. These activities have risen from the evolutionary pressure to detoxify haloaromatic compounds that are secreted by other infaunal marine organisms that co-inhabit the benthic ecosystem. Two isoenzymes of DHP, A and B, have been isolated and characterized.^{5, 12} The structural variations between them are limited to five amino acid substitutions: four are grouped in the distal (R32K and Y34N) and proximal (N81S and S91G) sides of the heme cofactor, with the fifth (I9L) located in a hydrophobic region of the enzyme without a direct contact to the heme cavity (Figure 2.1). These amino acid substitutions do not perturb the overall structural fold of DHP when comparing the two isoenzymes.²¹ However, they have resulted in DHP B exhibiting a 3-fold increase in enzyme turnover (k_{cat}) and a 1.8-fold increase in catalytic efficiency (k_{cat}/K_m) when compared to isoenzyme A for peroxidase activity, and a 2.2-fold increase for peroxygenase activity¹². In this study, substitutions of the five amino acids were probed sequentially and in combination in order to ascertain their effects on the structure-function relationships that discriminate peroxidase and peroxygenase activities between the two isoenzymes.

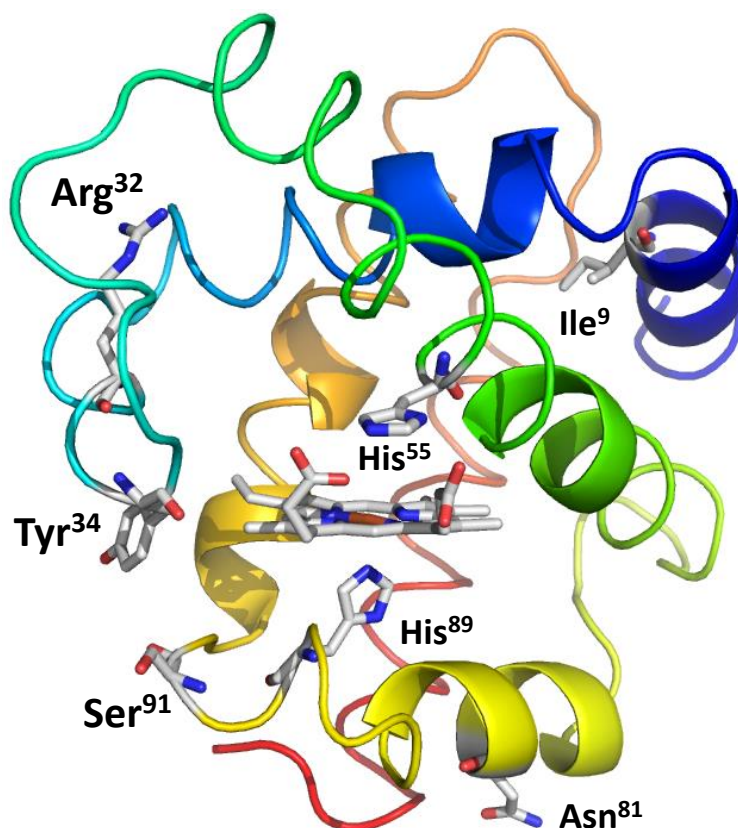


Figure 2.1. Dehaloperoxidase A (DHP A) (PDB: 4DWU). The heme group, the proximal and distal histidines (His89 and His55, respectively), and 5 amino acids that differ in DHP B are highlighted.

Experimental

Materials. HPLC grade acetonitrile (MeCN) and all other chemicals were purchased from VWR and Fisher Scientific. Unless otherwise specified, all chemicals were used without further purification. 1000X stock solutions of soybean trypsin inhibitor (STI) in ddH₂O, phenylmethylsulfonyl fluoride (PMSF) and N-*p*-Tosyl-L-phenylalanine chloromethyl ketone (TPCK) in EtOH were prepared prior to use. The enzyme concentration in the solution was determined spectrophotometrically using the molar absorptivity coefficient ($\epsilon_{406} = 116.4 \text{ M}^{-1} \text{ cm}^{-1}$)¹². Stock solutions (2 mM) of trichlorophenol (TCP) were prepared in 100 mM potassium phosphate (KPi) buffer (pH 7) and stored at -80 °C. Trichlorophenol concentration and lack of degradation was monitored by measuring its absorbance at 312 nm ($\epsilon = 3752 \text{ M}^{-1} \text{ cm}^{-1}$)¹². Stock

solutions (10 mM) of 5-haloindoles were prepared in MeOH, stored at -80 °C, and screened by HPLC for degradation prior to use. Solutions of H₂O₂ were prepared fresh and stored on ice while protected from light until needed. The concentration of H₂O₂ was determined spectrophotometrically ($\epsilon_{240} = 46 \text{ mM}^{-1} \text{ cm}^{-1}$)¹².

Construction of Mutant DHP Plasmids. Site-directed mutagenesis was performed using the Quikchange II site-directed mutagenesis kit (Agilent Technologies). Mutagenesis [melt (95 °C, 60 s), anneal (55 °C, 50 s), and extension (68 °C, 360 s)] was performed for 16 cycles. Oligonucleotides (Table 2.1) were synthesized by Integrated DNA Technologies (IDT). The plasmid encoding an N-terminal poly-His tag wild-type DHP A was used as a template for single mutations. Double and triple mutants were generated from preceding single and double mutants, respectively. The modified plasmids were transformed into BL21-Gold(DE3) competent cells (Agilent Technologies) and selected based on survival on LB-agar-ampicillin (100 µg/ml) plates. The plasmids were extracted using the spin column plasmid DNA kit (Bio Basic), and the desired mutation was confirmed by sequencing (Genewiz).

Table 2.1. Mutagenic Primers Used to Construct the DHP A Mutants.

Mutation	Forward Primer	Reverse Primer
A 19L	CAA GAT ATT GCC ACC <u>CTC</u> CGC GGT GAT CTC CGC	GCG GAG ATC ACC GCG <u>GAG</u> GGT GGC AAT ATC TTG
A R32K	G TAT CCG GAC GAG <u>AAA</u> CGC TAC TTC AAA AAC TAT G	C ATA GTT TTT GAA GTA GCG <u>TTT</u> CTC GTC CGG ATA C
A Y34N	CCG GAC GAG CGC CGC <u>AAC</u> TTC AAA AAC TAT GTC	GAC ATA GTT TTT GAA <u>GTT</u> GCG GCG CTC GTC CGG
A N81S	CTT GCG TCC GAC GCC <u>AGC</u> ACA CTC GTC CAG ATG	CAT CTG GAC GAG TGT <u>GCT</u> GGC GTC GGA CGC AAG
A S91G	G ATG AAA CAG CAT TCC <u>GGC</u> CTG ACG ACT GGA AAC	GTT TCC AGT CGT CAG <u>GCC</u> GGA ATG CTG TTT CAT C
A R32K/Y34N	CCG GAC GAG <u>AAA</u> CGC <u>AAC</u> TTC AAA AAC TAT GTC	GAC ATA GTT TTT GAA <u>GTT</u> GCG <u>TTT</u> CTC GTC CGG
A 19V	CAA GAT ATT GCC ACC <u>GTC</u> CGC GGT GAT CTC CGC	GCG GAG ATC ACC GCG <u>GAC</u> GGT GGC AAT ATC TTG
A 19A	CAA GAT ATT GCC ACC <u>GCC</u> CGC GGT GAT CTC CGC	GCG GAG ATC ACC GCG <u>GCC</u> GGT GGC AAT ATC TTG
A 19G	CAA GAT ATT GCC ACC <u>GGC</u> CGC GGT GAT CTC CGC	GCG GAG ATC ACC GCG <u>GCC</u> GGT GGC AAT ATC TTG

Protein Expression and Purification. A culture tube containing 10 mL of LB media was inoculated with 100 µL of starter culture containing 100 µg/mL of ampicillin, and

incubated in a shaker at 500 rpm for 12 hours at 37 °C. Each starter culture was used to inoculate a 1.5 L of LB media (4 flasks, 6 L total) containing 100 µg/mL ampicillin and 70 mg/L hemin (dissolved in 0.2 M NaOH). Cultures were incubated in an orbital shaker at 250 rpm for 8 hours at 37 °C. Protein overexpression was induced with 750 µM isopropyl β-D-1-thiogalactopyranoside (IPTG), and cells were further cultured at 250 rpm for 18 hours at 32 °C. A cell pellet was then obtained by centrifugation for 20 minutes at 3700 g and 4 °C, and subsequently stored in the -80 °C freezer.

Purification of the 6xHis-tag DHP protein was achieved by immobilized metal affinity (Ni^{2+}) followed by cation exchange chromatographies (CM-52). A cell pellet from 4 large growths collected in expression step was thawed. The cell pellet was then resuspended in 100 ml of an equilibration buffer (100 mM of sodium phosphate containing 20 mM imidazole at pH 8). Once the cell pellet was completely resuspended, it was transferred to a smaller plastic container in order to increase the depth of the solution for more effective sonication. While gently stirring on a stirrer plate at 4 °C, lysozyme (1 mg/mL) and protease inhibitors (soybean trypsin inhibitor (STI) (10 mg/mL), phenylmethylsulfonyl fluoride (PMSF) (75 mg/mL), *N*-*p*-Tosyl-L-phenylalanine chloromethyl ketone (TPCK) (10 mg/mL) and 1 mL of Triton X-100 (Bio Basic Canada Inc) were added to the suspension and stirred for an additional 20 minutes. In addition to chemical lysis, cells were subjected to sonication (Power 5, Cycle 50) for 5 cycles (3 min on/5 min off) while stirring on ice. Cell debris was removed by centrifugation for 1 hour at 16000 g at 4 °C. The cell pellet was discarded and the crude cell extract was collected into a clean centrifuge tube, and centrifuged for an additional 30 minutes at 16000 g at 4 °C. As needed, the solution was micron-filtered via a syringe filter to remove any remaining cell debris.

The crude protein solution was loaded onto two inline GE HisTrap (5 mL) purification columns (pre-equilibrated with 5 volumes of equilibration buffer) at a flow rate of 3 mL/minute. The columns were washed with a 100 mM sodium phosphate buffer containing 20 mM imidazole and 0.5 M NaCl (pH 8) until the eluent was mostly clear. Protein was eluted with 100 mM sodium phosphate containing 200 mM imidazole and 0.5 M NaCl (pH 8). The protein was then oxidized to a homogeneous solution of the ferric form of the enzyme with the

addition of potassium ferricyanide ($K_3[Fe(CN)_6]$) until a slight color change was noticed (~ 5 min), followed by 3 x 4L of dialysis in against 10 mM KP_i buffer (pH 7) at 4 °C performed over 24 h using 12-14 kDa MWCO membrane tubing (Spectra/Por, VWR). After dialysis, the crude protein was centrifuged for 20 minutes at 3700 g at 4 °C to remove any precipitated material. Cation exchange chromatography was then performed using CM-52 stationary phase (Whatman) that was wet packed into a column (10 mm (ID) x 200 mm (L), 16 mL) that was pre-equilibrated with 5 volumes of 5 mM KP_i (pH 7). The protein solution was loaded and subsequently washed with 10 mM KP_i (pH 7) at 1.5 mL/min until all minor fractions were removed. Protein was eluted with 38 mM KP_i (pH 7). Fractions that exhibited a Reinheitszahl value, $Rz (Abs_{soret}/Abs_{278}) \geq 4.0$ were collected, brought to 40% (v/v) glycerol, and stored at -80 °C.

Molecular Weight Determination. The molecular weights of the proteins utilized in the experiments were determined via Thermo Fisher Scientific Exactive Plus MS using a Heated Electrospray Ionization (HESI) and operated in positive ion mode. The protein samples were prepared in 100 mM KP_i at pH 7. The mobile phase was 90:10 methanol with 0.1% formic acid (v/v): water. The experimentally determined and calculated monomeric molecular weights of the dehaloperoxidase mutants were summarized in Table 2.2.

Table 2.2. Calculated monomeric molecular weights and experimentally determined weights of the dehaloperoxidase mutants.

Protein	Calculated mass (Da)	Measured Mass (Da)
DHP A WT	16408.51	16408.09
DHP B WT	16274.38	16274.38
I9L	16408.51	16408.03
R32K	16380.50	16380.05
Y34N	16359.44	16359.04
N81S	16381.48	16381.07
S91G	16378.49	16378.03
I9V	16394.49	16394.04
I9L/R32K	16380.50	16380.05
I9L/Y34N	16359.44	16359.04
I9L/N81S	16381.48	16381.01
I9L/S91G	16378.49	16378.03
R32K/Y34N	16331.43	16331.02
R32K/N81S	16353.47	16353.05
R32K/S91G	16350.48	16350.04
Y34N/N81S	16332.41	16332.03
Y34N/S91G	16329.42	16329.03
N81S/S91G	16351.46	16351.04
I9L/R32K/Y34N	16331.43	16331.04
I9L/R32K/N81S	16353.47	16353.02
I9L/R32K/S91G	16350.48	16350.00
I9L/Y34N/N81S	16332.41	16332.02
I9L/Y34N/S91G	16329.42	16329.03
I9L/N81S/S91G	16351.46	16351.03
R32K/Y34N/N81S/S91G (B L9I)	16274.38	16273.99

Preparation of Ferric DHP. Purified DHP was treated with an excess of potassium ferricyanide in order to obtain a homogeneous solution in the ferric state. After 2 minutes, ferri/ferrocyanide was removed using a PD-10 desalting column (GE Healthcare). Eluted protein was concentrated with Amicon Ultra Centrifugal Filter (EMD Millipore) equipped with 10 kDa MWCO membrane.

Peroxidase Studies. The hydrogen peroxide-dependent oxidative dehalogenation of 2,4,6-trichlorophenol (TCP) catalyzed by DHP was measured on Cary 50 UV-vis spectrophotometer. The reaction with TCP yielded a 2,6-dichloro-1,4-benzoquinone (DCQ) product with peak absorbance at 273nm. The reactions were performed in triplicate at pH 7 in 100 mM KP_i at 25 °C. Buffered solutions of DHP and TCP were premixed and the reaction was initiated by the addition of H_2O_2 (1 mL total volume). Final concentrations were 0.5 μM DHP, 150 μM TCP, and 10, 25, 50, 75, 100, or 125 μM H_2O_2 . The change in absorbance at 312 nm (λ_{max} of TCP) was measured using Cary WinUV Kinetics software over a 30 second time frame with rate of 1 scan per second. Using a known ϵ value for TCP ($3752 \text{ M}^{-1} \text{ cm}^{-1}$), measured slope was converted to $-\text{d}[\text{TCP}]/\text{d}t$. The data were fit to standard Michaelis-Menten kinetics using the method of initial rates in the Grafit software package (Erithacus Software). The kinetics parameters K_m and k_{cat} resulted from the optimization of the fitting procedure.

Peroxygenase Studies. The percent conversion of 5-Br-indole due to hydrogen peroxide-dependent oxidation catalyzed by DHP was analyzed by HPLC using a Waters 2796 Bioseparations Module coupled with a Waters 2996 Photodiode Array Detector and equipped with an ODS Hypersil C_{18} column (Thermo-Scientific, 150 mm x 4.6 mm, 5 μm particle size). The reactions were performed in triplicate in 100 mM KP_i at pH 7 in 5% MeOH at 25 °C. Buffered solutions of 5-Br-indole and DHP were premixed, and the peroxygenase reaction was initiated with addition of H_2O_2 . Final concentrations were 10 μM DHP, 5-500 μM Br-indole and 500 μM H_2O_2 in 250 μL total volume. After 5 minutes of incubation at 25 °C, the reaction was quenched with excess catalase (150 units). A 100 μL aliquot of the reaction was then diluted with 900 μL of 100 mM KP_i at pH 7 (1:10 dilution). 200 μL of the diluted sample was subjected to HPLC analysis (solvent A, dd H_2O containing either 0.1% or 1% of trifluoroacetic acid; solvent B, MeCN). The elution method was as follows: 1.5 mL/min of 95:5 (A:B) to 5:95 using a linear gradient over 10 min; 5:95 isocratic for 2 minutes; 5:95 to 95:5 using a linear gradient over 1 min, and then isocratic for 4 min. Analysis was performed using the Empower software package (Waters Corp.). A non-enzymatic control was utilized for the calculation of percent conversion of 5-Br-indole ($t_r = 7.9$ min) against a calibration curve generated using serial dilutions.

Stopped-Flow UV-visible Studies. Experiments were performed using a Bio-Logic SFM-400 triple-mixing stopped-flow instrument interfaced to a rapid scan diode array UV-visible spectrophotometer. All the solutions were prepared in 100 mM KP_i at pH 7 and all of the experiments were performed at room temperature. Single mixing experiments reacting enzyme and H_2O_2 with final concentrations of 10 μM and 100 μM , respectively were performed to observe spectral features and rate constants of Compound ES and Compound RH formation. Spectra (900 scans) were collected over three time-domain regimes (2, 25 and 250 ms; 300 scans each) using Bio Kinet32 software package (Bio-Logic). All data were evaluated using Specfit Global Analysis System software (Spectrum Software Associates) and fit by SVD analysis as two-step, three species irreversible mechanism.

5-Br-indole Binding Studies. The 5-Br-indole dissociation constant (K_d) was measured using a Cary 50 UV-vis spectrophotometer. A stock solution of 10 mM 5-Br-indole in MeOH was prepared in a glass vial. The measurements were performed in triplicate in 100 mM KP_i at pH 7 in 10% MeOH at 25 °C. The UV-vis spectrophotometer was referenced with 10 μM ferric DHP in 100 mM KP_i (pH 7) containing 10% MeOH (v/v). The total volume of the samples was 200 μl with final concentrations of 10 μM ferric DHP and either 31.25, 62.5, 125, 250, 500 or 1000 μM 5-Br-indole while maintaining 10% MeOH (v/v). Perturbations in absorbance at the Soret region (ΔA) were recorded for each 5-Br-indole concentration. Analysis by nonlinear regression⁴⁵ provided a calculated A_{max} , which was used to calculate α ($\Delta A/\Delta A_{\text{max}}$) for the average ΔA for each concentration. In addition, the nonlinear regression plot provided the reported K_d values.

Resonance Raman Studies. Resonance Raman studies were performed by Soret band excitation using a Coherent Mira 900 titanium sapphire (Ti:sapphire) laser. The Ti:sapphire laser was pumped using a Coherent Verdi 10 frequency doubled diode pumped neodymium-doped vanadate (Nd:vanadate) laser producing 10 W at 532 nm. The beam generated was sent through a Coherent 5-050 doubler to generate a normal working range of 400-430 nm laser sufficient for Soret band excitation of DHP and DHP/indole complexes. Generated laser power at the sample was 60 mW. Additionally, the beam was collimated and cylindrically focused to a vertical line of ≈ 0.5 mm on the sample. Scattered light was collected with Spex 1877 triple

spectrophotometer equipped with a liquid nitrogen-cooled CCD detector. Spectra were collected and analyzed by Spectramax software. Total volume of the samples was 200 μL with final concentrations of 100 μM (DHP) and 1 mM (5-Br-indole or 5-I-indole) in 100 mM KPi (pH 7) containing 10% MeOH (v/v). Samples were premixed in a 2 mL tube and transferred to 5 mm diameter glass NMR tube. Spectra were collected over 20 minutes with 30 seconds per scan and collected data was calibrated and graphed using Igor Pro (WaveMetrics).

Results and Discussion

UV-Visible Spectra of the Mutants in the Resting (Fe^{3+} Heme) State. The obtained spectra of the oxidized heme proteins are typical of high spin ferric heme forms ($S = 5/2$); their optical characteristics, optical purity ratio (A_{Soret}/A_{278} , R_z), and the ratio of absorbances A_{Soret}/A_{380} and A_{614}/A_{645} of the two WT DHP isoenzymes, DHP A single, double, I9L triple mutants and DHP A (R32K/Y34N/N81S/S91G) (B L9I) are detailed in Table 2.3. The ratio of A_{Soret}/A_{380} and A_{614}/A_{645} are used to estimate a relative proportion of the five- and six-coordinate high spin ferric heme populations; the greater the ratios, the greater the six-coordinate to five-coordinate population ratio.⁴⁶⁻⁴⁸ The Table 2.4. details change in optical characteristics and estimated percentage of oxyferrous forms of WT DHP A, WT DHP B, DHP A (I9L), DHP A (Y34N), DHP A (S91G), DHP A (I9L/Y34N), DHP A (I9L/S91G), DHP A (Y34N/S91G), DHP A (I9L/Y34N/S91G) and DHP A (R32K/Y34N/N81S/S91G) (B L9I) during 360 hour scans in aerobic environment. The estimated percentage of oxyferrous form in the solution was calculated by comparing Q-band region to a linear combination of Q-band regions of ferric and oxyferrous DHP A WT.

The optical spectra of the two WT DHP isoenzymes and DHP A (I9L) are shown in Figure 2.2. The WT DHP A exhibited spectroscopic changes during 360 hours in aerobic conditions with bathochromic shift of Soret band and appearance of oxyferrous bands in Q-band regions (Soret: 407 nm to 409 nm; Q-bands: 538 nm, 578nm), (Figure 2.9). These changes correspond to increase in oxyferrous form of the enzymes from ~0% to ~20%. Similarly to WT DHP A, WT DHP B enzyme exhibited changes in Soret band and Q-band regions (Soret: 407 nm to 409 nm; Q-bands: 538 nm, 574 nm), (Figure 2.10.). The estimated

concentration of oxyferrous form of the enzymes increased from ~5% to ~20%. The DHP A (I9L) mutant exhibited the lowest observed A_{Soret}/A_{380} and A_{614}/A_{645} ratios (1.77 and 0.97) indicating a greater relative proportion of the five-coordinated ferric heme population when compared to the other proteins. However, it exhibited significant changes in spectroscopic features over 360 hours in aerobic conditions corresponding to increase in oxyferrous form from ~0% to ~30%, shown in Figure 2.11. The spectrum of DHP A (I9L) after 360 hours displayed a bathochromic shift of the Soret band (406 nm to 410 nm) and appearance of oxyferrous Q-band features (539 nm and 577 nm). In contrast, the DHP A (Y34N) mutant (Figure 2.3.) displayed the highest ratios out of the single mutants (2.05 and 1.39), which indicated a greater relative proportion of the six-coordinated ferric heme population. The spectrum of DHP A (Y34N) contained ~15% of oxyferrous form of the enzyme. The presence of oxyferrous form enzyme was confirmed by resonance Raman spectroscopy discussed later in the chapter. The DHP A (Y34N) mutant exhibited moderate changes in spectroscopic features over 360 hours (Soret: 408 nm to 409 nm; Q-bands: 538 nm, 572 nm), (Figure 2.12.). The estimated oxyferrous form of the enzyme increased from ~15% to ~25%. The DHP A (S91G) spectrum displayed 2nd lowest ratios out of the single mutants after DHP A (I9L) (1.91 and 1.04 vs 1.77 and 0.97) with ~0% estimated oxyferrous form of the enzyme. During 360 hour scan, DHP A (S91G) displayed minor changes in spectroscopic features (Soret: 406 nm to 407 nm; Q-bands: 534 nm, 577 nm), (Figure 2.13.). These changes correspond to increase in presence of oxyferrous form of the enzyme from 0% to 5%. This a significant difference in concentration of oxyferrous form of the enzyme between DHP A (I9L) and DHP A (S91G) after 360 hours scan (~30% vs ~5%).

The optical spectra of DHP A mutants I9L/R32K, I9L/Y34N, I9L/N81S, and I9L/S91G are shown in Figure 2.4. DHP A (I9L/Y34N) exhibited the highest ratios out of the I9L double mutants (1.95 and 1.19), and displayed a uniquely similar optical spectrum to that of the DHP A (Y34N) mutant with ~15% of oxyferrous form of the enzyme. However, the addition I9L substitution to the DHP A (Y34N) mutant increased the five-coordinate ferric heme population, indicated by the decrease in A_{Soret}/A_{380} and A_{614}/A_{645} ratios (1.95, 1.19 vs 2.05, 1.39). Interestingly, DHP A (I9L/Y34N) displayed a largest bathochromic shift in Soret band and

enhancement of oxyferrous Q-bands (Soret: 408 nm to 418 nm; Q-bands: 540 nm, 575 nm), (Figure 2.14.). These spectroscopic changes represented a significant increase in oxyferrous form of the enzyme from ~15% to ~40%. In addition, removal of I9L substitution from WT DHP B generated DHP A (R32K/Y34N/N81S/S91G) (B L9I) mutant which displayed an increase of A_{Soret}/A_{380} and A_{614}/A_{645} ratios (1.91, 1.06 vs 1.98, 1.36) that corresponds to a decrease of five-coordinate ferric heme population. The optical spectra of B (L9I) closely resembles the optical spectra of WT DHP B shown in Figure 2.2. The estimated oxyferrous content of WT DHP B and B (L9I) was ~5% for both enzymes. Presence of oxyferrous form of the enzyme increased from ~5% to ~25% over 360 hours scan, represented by a bathochromic shift of the Soret band and enhancement of oxyferrous Q-bands (Soret: 407 nm to 411nm; Q-bands: 539 nm, 578 nm), (Figure 2.18.). The combination of I9L and S91G resulted in the highest population of five-coordinate ferric heme (1.80 and 1.03) with estimated concentration of oxyferrous form of the enzyme at ~0%. Even after 360 hours in aerobic conditions, there was no detectable change in presence of oxyferrous form of the enzyme. The DHP A (I9L/S91G) did not exhibit bathochromic shift of the Soret band (406 nm) and minor changes in the Q-band region (577 nm), (Figure 2.15.).

The optical spectra of the DHP A mutants R32K/Y34N, R32K/N81S, R32K/S91G, Y34N/N81S, Y34N/S91G and N81S/S91G are presented in Figure 2.5. Similar to the DHP A (Y34N) and DHP A (I9L/Y34N) mutants, the addition of the Y34N mutation to DHP A (R32K) and DHP A (N81S) yielded an increase in six-coordinate population indicated by increase in the A_{Soret}/A_{380} and A_{614}/A_{645} ratios (2.16, 1.46 vs 1.96, 1.08 and 2.12, 1.40 vs 2.00, 1.10). Additionally, the optical spectra of DHP A (R32K/Y34N) and DHP A (Y34N/N81S) contained ~25% and ~20% of oxyferrous form, respectively. However, the addition of the Y34N substitution to DHP A (S91G) did not result in a significant deviation of the optical spectrum compared to DHP A (S91G), nor did it result in a significant increase in the six-coordinate ferric heme population (1.95, 1.23 vs 1.91, 1.04) and showed ~5% of oxyferrous form of DHP. In DHP A (Y34N/S91G), the concentration of oxyferrous form of the enzyme increased from ~5% to ~20% during 360 hour scan with minor bathochromic shift of the Soret band and

enhancement of oxyferrous bands in Q-band region (Soret: 407 nm to 408 nm; Q-bands: 537 nm, 577 nm), (Figure 2.16.).

The optical spectra of the DHP A I9L triple mutants I9L/R32K/Y34N, I9L/R32K/N81S, I9L/R32K/S91G, I9L/Y34N/N81S, I9L/Y34N/S91G, and I9L/N81S/S91G are shown in Figure 2.6. A similar pattern established in the double mutants containing the I9L, Y34N, and S91G mutations is observed in the I9L triple mutants. Addition of the I9L substitution to DHP A (R32K/Y34N) increases the five-coordinate population indicated by decrease in A_{Soret}/A_{380} and A_{614}/A_{645} ratios (2.16, 1.46 vs 2.06, 1.21), and a decrease in the amount of oxyferrous form of the enzyme from ~25% to ~20%. A similar effect is observed in DHP A (I9L/Y34N/N81S) compared to DHP A (Y34N/N81S) (1.96, 1.13 vs 2.12, 1.40) and a similar decrease in oxyferrous content from ~20% to ~15%. Combination of I9L and Y34N/S91G displayed a similar trend by lowering A_{Soret}/A_{380} and A_{614}/A_{645} ratios (1.95, 1.23 vs 1.86, 1.11) and decreasing the percentage of oxyferrous content from ~5% to ~0% compared to DHP A (Y34N/S91G). The spectrum of DHP A (I9L/Y34N/S91G) closely resembles a purely ferric spectrum of DHP A WT. The spectroscopic features exhibited minor changes during 360 hour scan. The Soret band displayed a slight bathochromic shift and appearance of oxyferrous features in the Q-band region (Soret: 406 nm to 407 nm; Q-bands: 538 nm, 576 nm), (Figure 2.17.). The estimated concentration of oxyferrous form of the enzyme increased from ~0% to ~15% over 360 hour period.

The pattern suggests that the addition of the Y34N mutation has a stabilizing effect on the six-coordinate ferric heme population and increases the percentage of oxyferrous form of the enzyme in the solution by stimulating the reduction of the enzyme (Figure 2.7). However, I9L and S91G mutations have a stabilizing effect on the five-coordinate ferric heme population and counteract the effect of Y34N substitution by stabilizing ferric form of the enzyme and in turn reducing the concentration of oxyferrous form of the enzyme present in the solution. Interestingly, the presence of the I9L substitution increases the rate of reduction of the enzyme and formation of oxyferrous form of the enzyme, demonstrated by DHP A (I9L) and DHP A (I9L/Y34N) mutants over 360 hour scan. However, the mutants containing S91G substitution displayed a decrease in rate of formation of oxyferrous form of the enzyme compared to

mutants lacking S91G substitution (WT DHP A vs DHP A (S91G), DHP A (I9L) vs DHP A (I9L/S91G), DHP A (Y34N) vs DHP A (Y34N/S91G)), (Table 2.4.). The effects of addition of Y34N substitution to single and double mutations are presented in Figure 2.8. The enzymes that contain Y34N mutation, but lack I9L and/or S91G mutation have the highest six-coordinate heme population represented by the greatest A_{Soret}/A_{380} and A_{614}/A_{645} ratios.

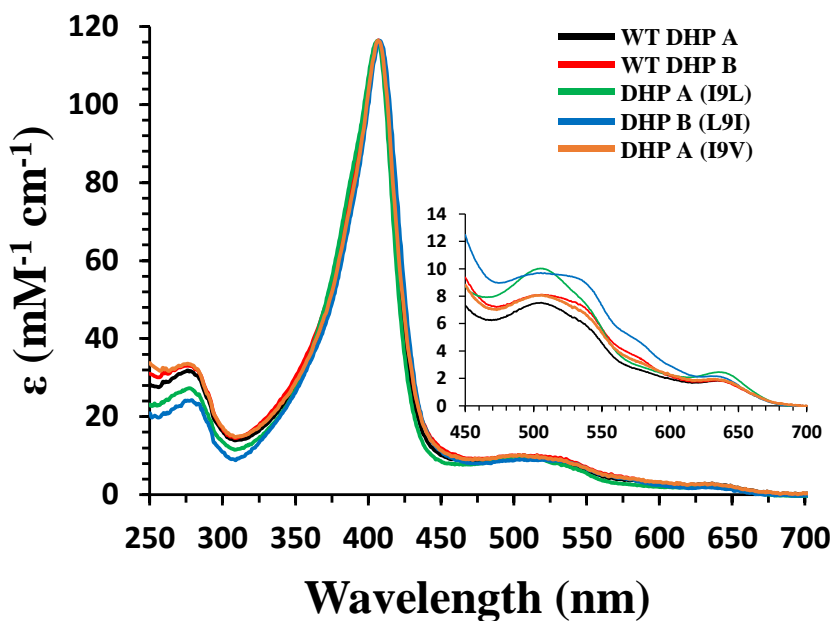


Figure 2.2. The UV-visible spectra of WT DHP A, WT DHP B, DHP A (I9L), DHP B (L9I) and DHP A (I9V) at pH 7.

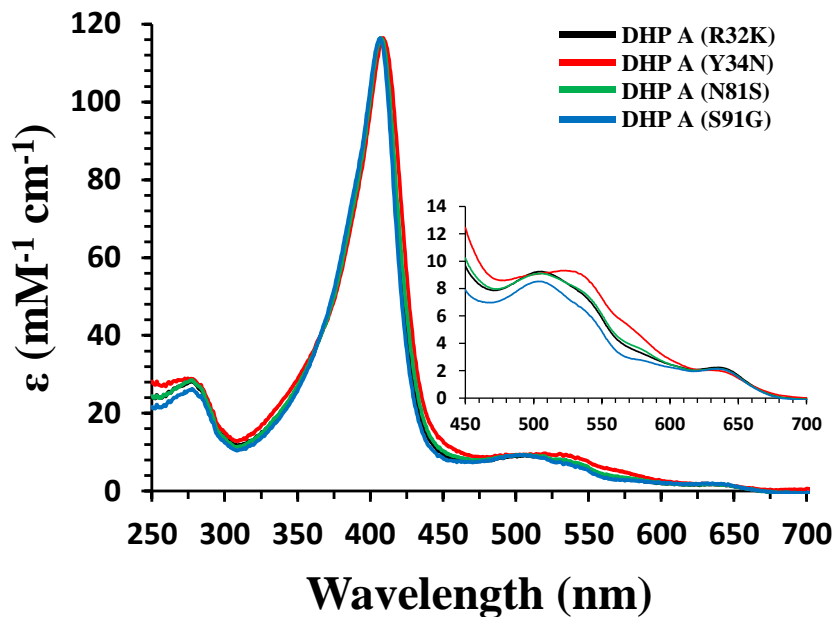


Figure 2.3. The UV-visible spectra of DHP A (R32K), DHP A (Y34N), DHP A (N81S) and DHP A (S91G) at pH 7.

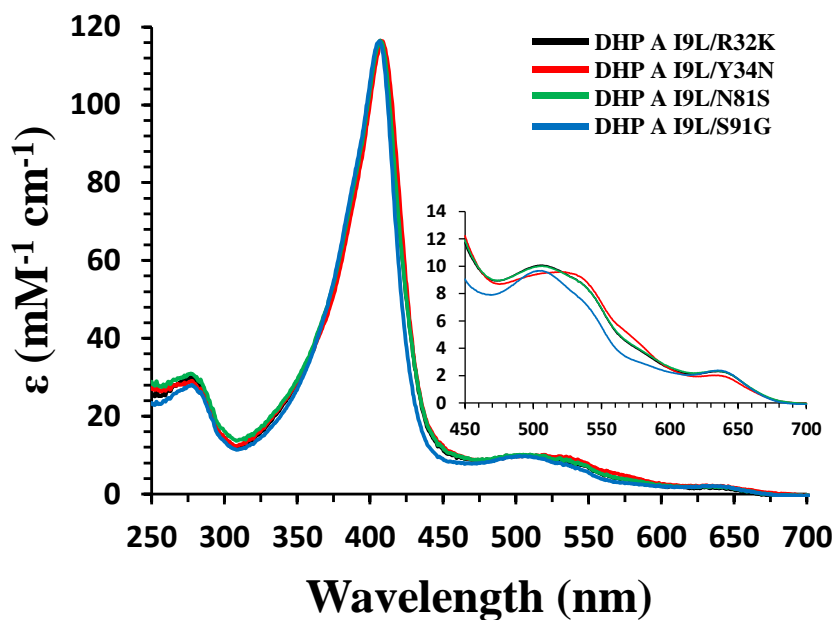


Figure 2.4. The UV-visible spectra of DHP A (I9L/R32K), DHP A (I9L/Y34N), DHP A (I9L/N81S) and DHP A (I9L/S91G) at pH 7.

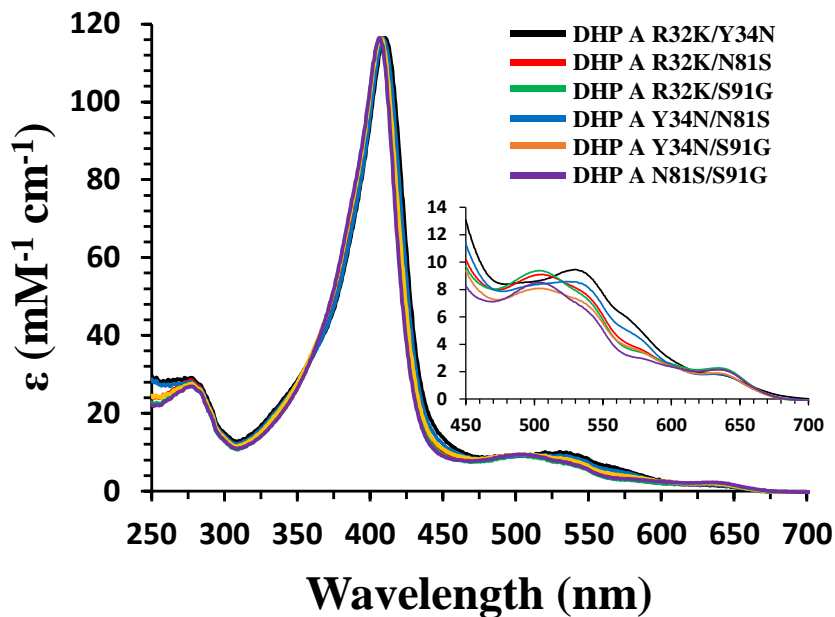


Figure 2.5. The UV-visible spectra of DHP A (R32K/Y34N), DHP A (R32K/N81S), DHP A (R32K/S91G), DHP A (Y34N/N81S), DHP A (Y34N/S91G) and DHP A (N81S/S91G) at pH 7.

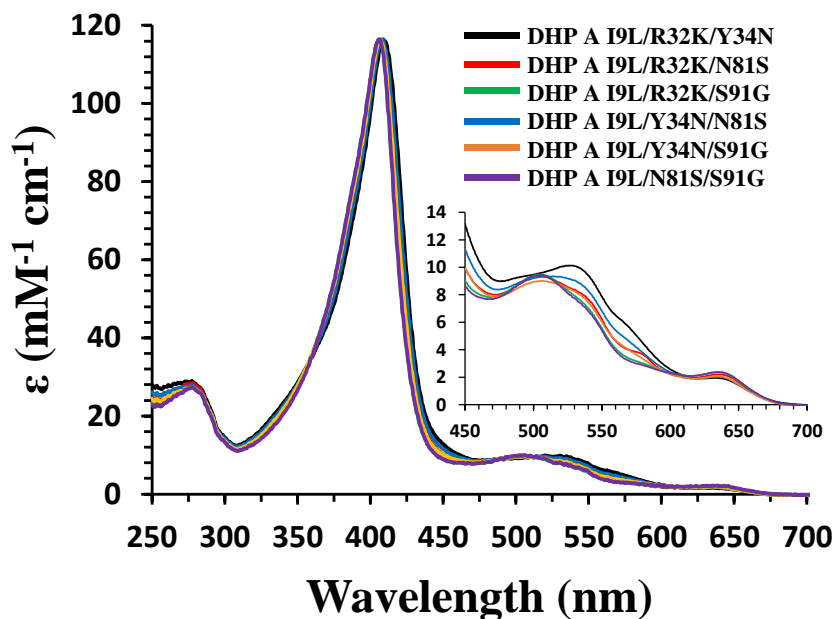


Figure 2.6. The UV-visible spectra of DHP A (I9L/R32K/Y34N), DHP A (I9L/R32K/N81S), DHP A (I9L/R32K/S91G), DHP A (I9L/Y34N/N81S), DHP A (I9L/Y34N/S91G) and DHP A (I9L/N81S/S91G) at pH 7.

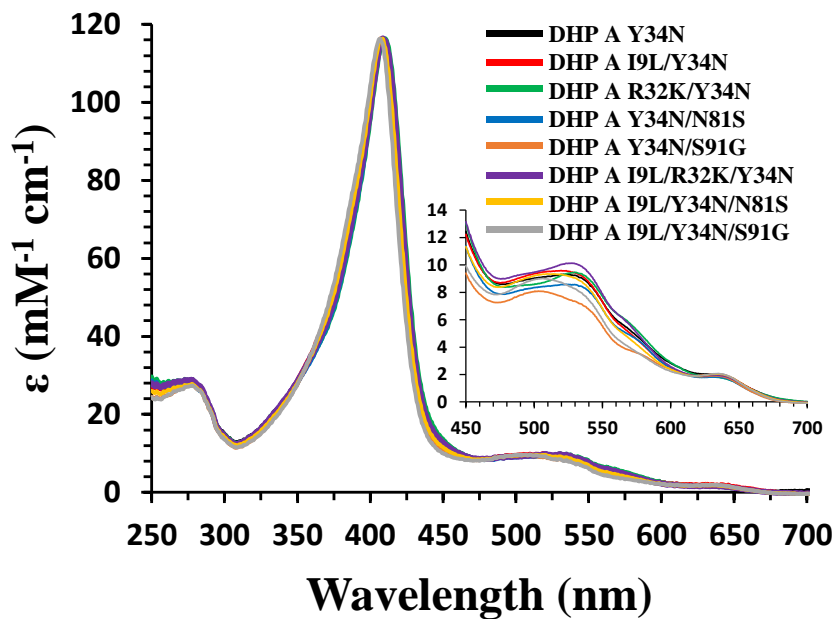


Figure 2.7. The UV-visible spectra of DHP A (Y34N), DHP A (I9L/Y34N), DHP A (R32K/Y34N), DHP A (Y34N/N81S), DHP A (Y34N/S91G), DHP A (I9L/R32K/Y34N), DHP A (I9L/Y34N/N81S) and DHP A (I9L/Y34N/S91G) at pH 7.

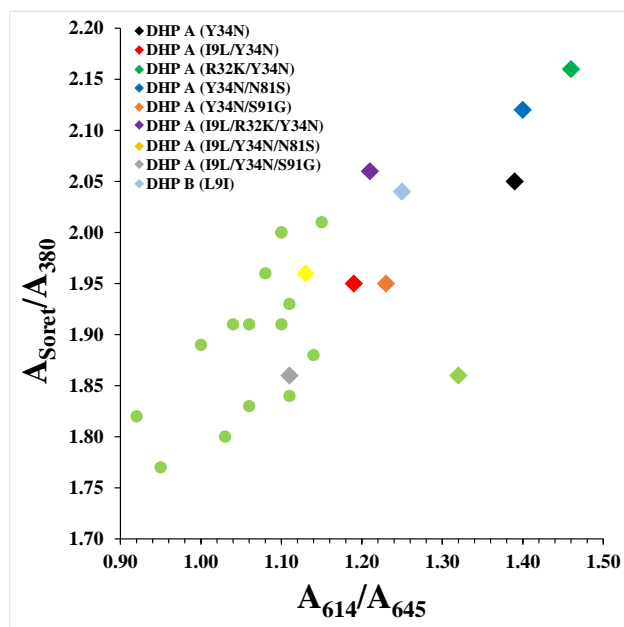


Figure 2.8. Scatter plot of A_{Soret}/A_{380} vs A_{614}/A_{645} of DHP enzymes listed in Table 2.3.

Table 2.3. UV-visible spectroscopic features of the DHP A variants and DHP B in the ferric heme state at pH 7.

Protein	λ_{\max} (nm)	A_{Soret}/A_{380}	A_{614}/A_{645}	R_z
WT DHP A	407, 506, 535 (sh), 635	1.91	1.06	4.41
WT DHP B	407, 506, 531 (sh), 633	1.88	1.14	4.13
I9L	406, 506, 535 (sh), 636	1.77	0.95	4.28
R32K	407, 506, 535 (sh), 635	1.96	1.08	4.16
Y34N	409, 494 (sh), 524, 556 (sh), 629	2.05	1.39	4.06
N81S	407, 505, 527 (sh), 634	2.00	1.10	4.13
S91G	407, 505, 528 (sh), 634	1.91	1.04	4.48
I9V	407, 507, 530 (sh), 633	2.01	1.15	3.93
I9L/R32K	407, 505, 530 (sh), 635	1.86	1.32	3.92
I9L/Y34N	408, 494 (sh), 523, 559 (sh), 633	1.95	1.19	4.04
I9L/N81S	407, 505, 530 (sh), 635	1.84	1.11	3.79
I9L/S91G	406, 504, 528 (sh), 635	1.80	1.03	4.20
R32K/Y34N	410, 496 (sh), 530, 556 (sh), 629	2.16	1.46	4.02
R32K/N81S	407, 506, 525 (sh), 634	2.00	1.10	4.13
R32K/S91G	407, 505, 524 (sh), 634	1.93	1.11	4.32
Y34N/N81S	408, 495 (sh), 530, 558 (sh), 630	2.12	1.40	4.21
Y34N/S91G	407, 504, 525 (sh), 634	1.95	1.23	4.25
N81S/S91G	407, 503, 527 (sh), 634	1.91	1.10	4.33
I9L/R32K/Y34N	408, 500 (sh), 527, 557 (sh), 632	2.06	1.21	4.06
I9L/R32K/N81S	407, 505, 525 (sh), 636	1.89	1.00	4.11
I9L/R32K/S91G	406, 504, 525 (sh), 636	1.83	1.06	4.25
I9L/Y34N/N81S	408, 492 (sh), 511, 555 (sh), 634	1.96	1.13	4.21
I9L/Y34N/S91G	407, 507, 525 (sh), 634	1.86	1.11	4.27
I9L/N81S/S91G	406, 505, 526 (sh), 636	1.82	0.92	4.28
R32K/Y34N/N81S/S91G	407, 492 (sh), 536 (sh), 570 (sh), 638	1.98	1.36	4.88

R_z , Reinheitszahl value. sh indicates “shoulder”

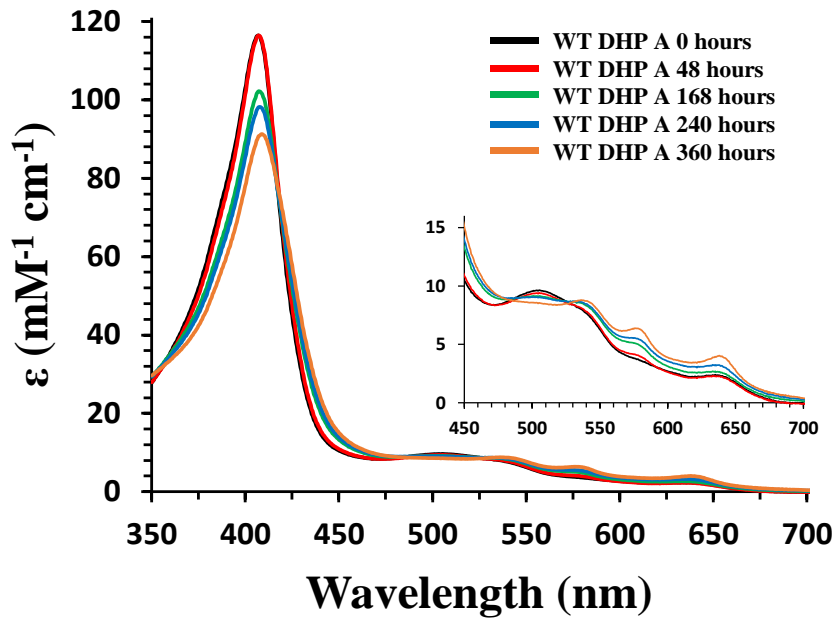


Figure 2.9. The UV-visible spectra of WT DHP A in aerobic conditions over 360 hours at pH 7.

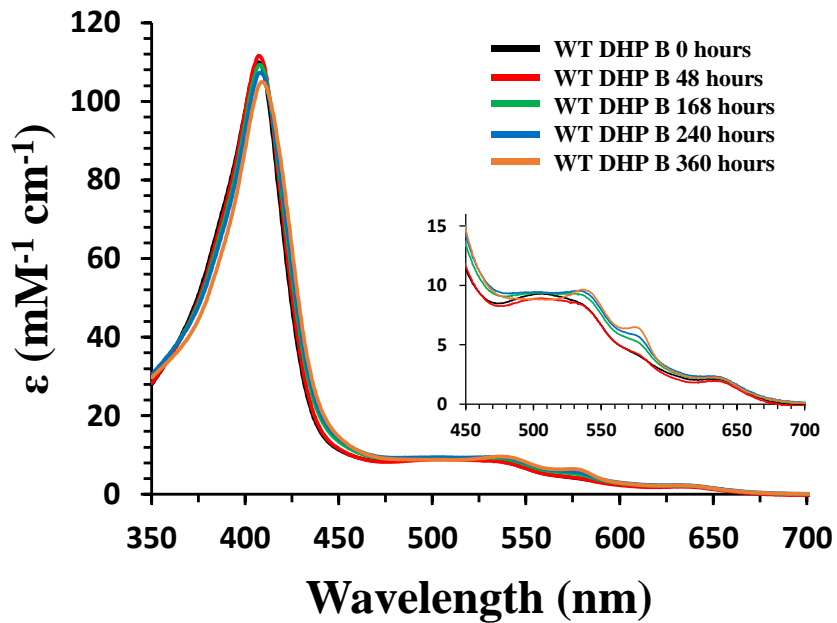


Figure 2.10. The UV-visible spectra of WT DHP B in aerobic conditions over 360 hours at pH 7.

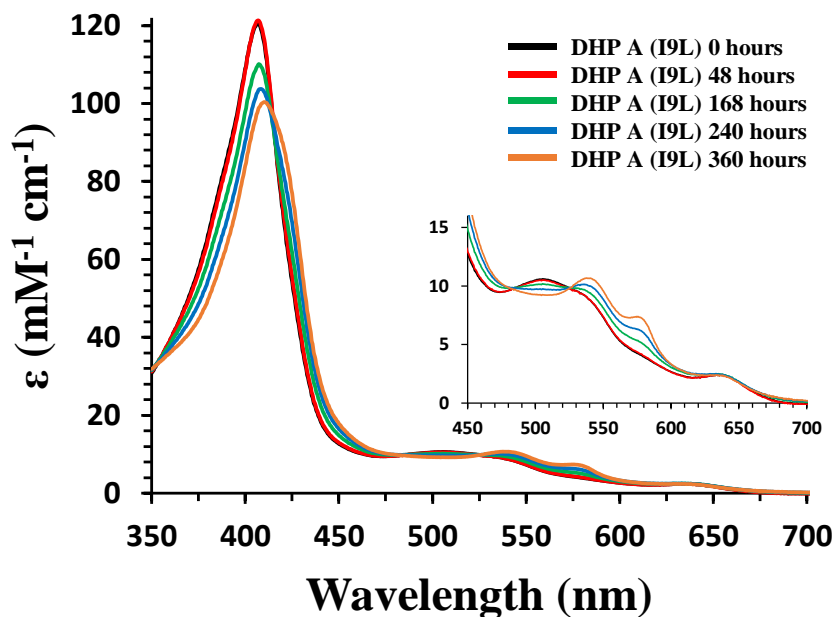


Figure 2.11. The UV-visible spectra of WT DHP A (I9L) in aerobic conditions over 360 hours at pH 7.

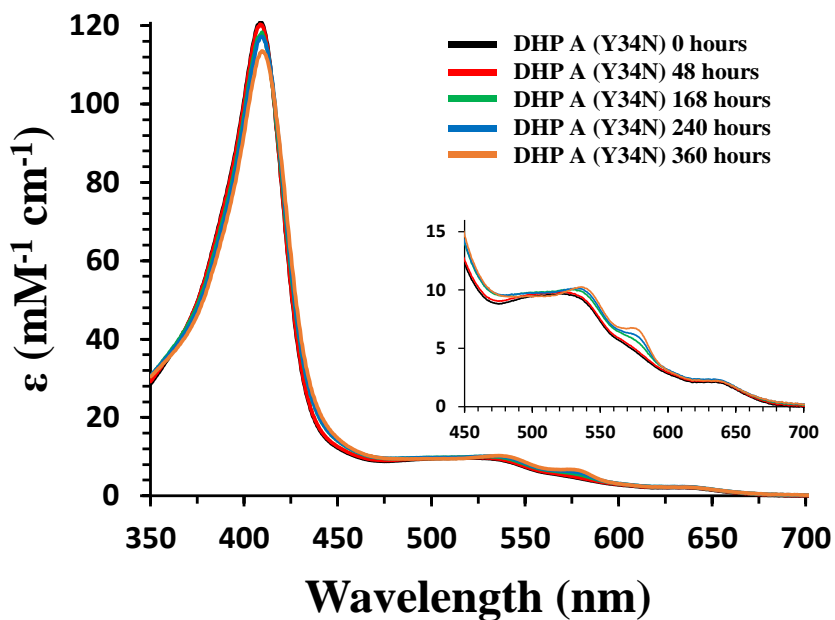


Figure 2.12. The UV-visible spectra of WT DHP A (Y34N) in aerobic conditions over 360 hours at pH 7.

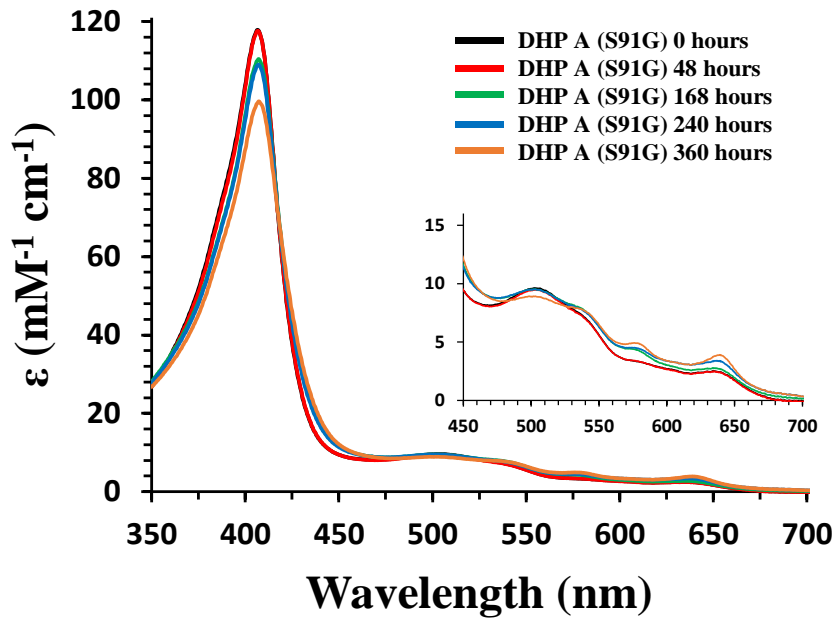


Figure 2.13. The UV-visible spectra of WT DHP A (S91G) in aerobic conditions over 360 hours at pH 7.

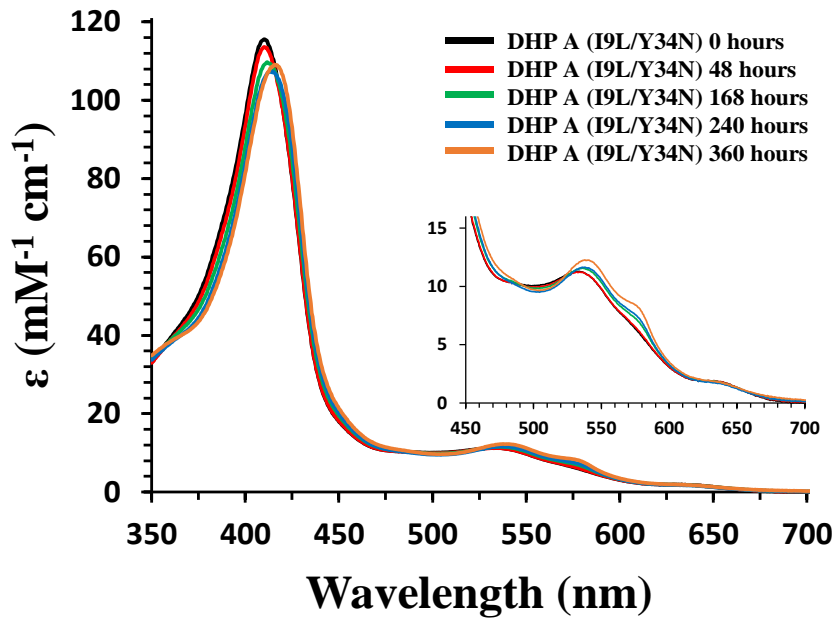


Figure 2.14. The UV-visible spectra of WT DHP A (I9L/Y34N) in aerobic conditions over 360 hours at pH 7.

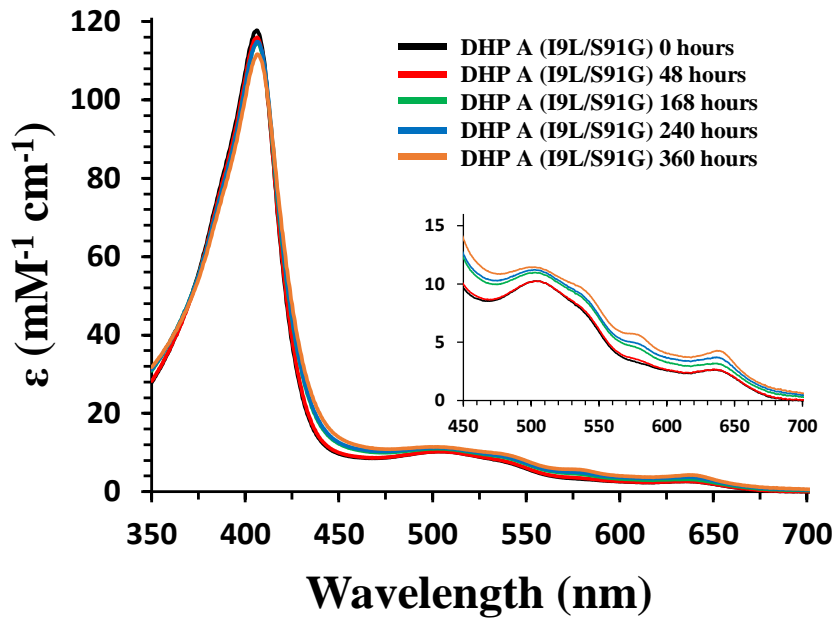


Figure 2.15. The UV-visible spectra of WT DHP A (I9L/S91G) in aerobic conditions over 360 hours at pH 7.

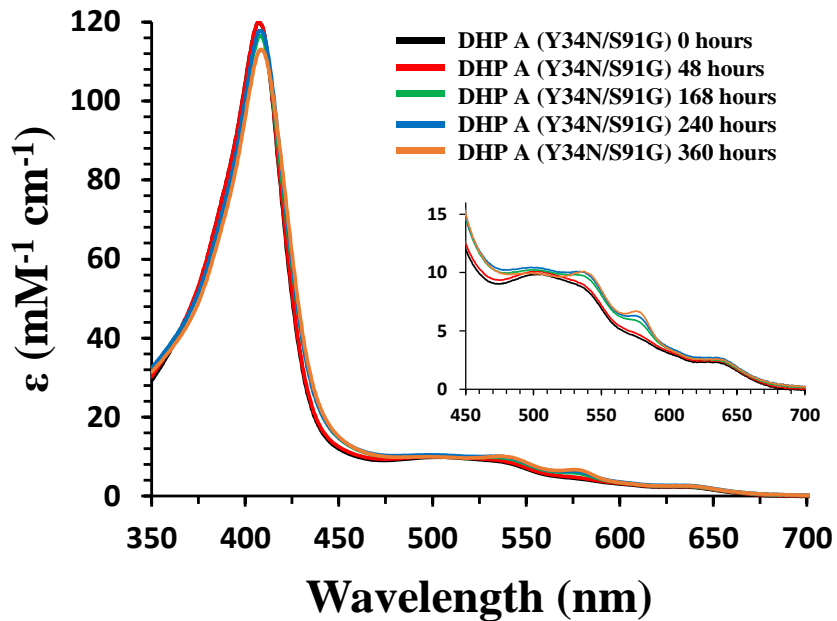


Figure 2.16. The UV-visible spectra of WT DHP A (Y34N/S91G) in aerobic conditions over 360 hours at pH 7.

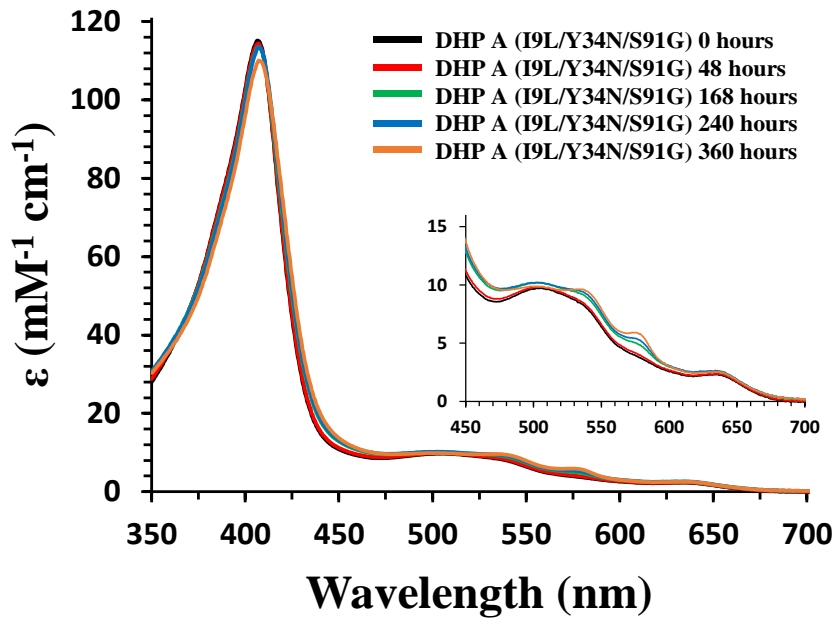


Figure 2.17. The UV-visible spectra of WT DHP A (I9L/Y34N/S91G) in aerobic conditions over 360 hours at pH 7.

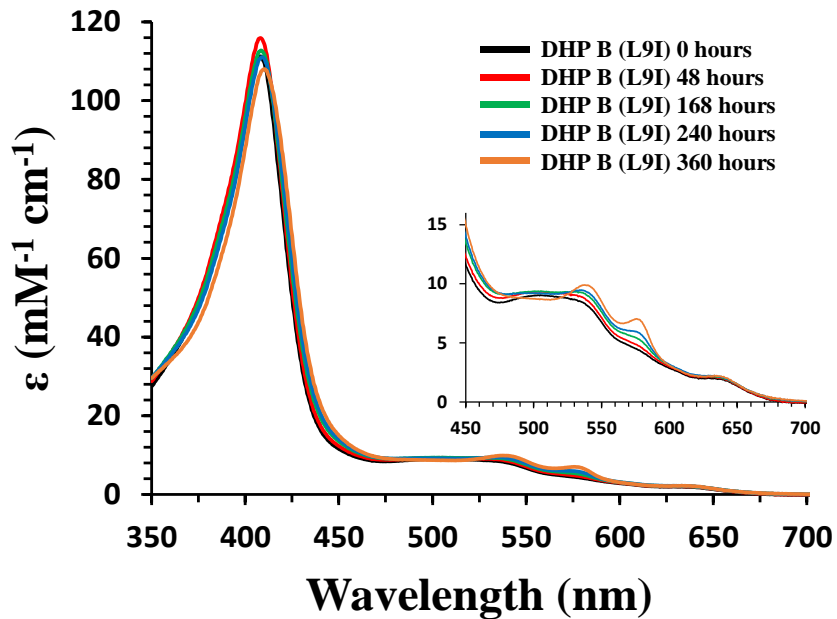


Figure 2.18. The UV-visible spectra of WT DHP B in aerobic conditions over 360 hours at pH 7.

Table 2.4. UV-visible spectroscopic features and estimated oxyferrous form of the DHP A variants and DHP B over 360 hours at pH 7.

Enzyme	Initial (0 hours)	Final (360 hours)	Estimated Oxyferrous Form (%)	
	Spectroscopic Features	Spectroscopic Features	Initial	Final
WT DHP A	407, 506, 535 (sh), 635	409, 538, 578, 638	0	20
WT DHP B	407, 506, 531 (sh), 633	409, 538, 574, 638	5	20
I9L	406, 506, 535 (sh), 636	410, 539, 574, 635	0	30
Y34N	409, 494 (sh), 524, 556 (sh), 629	409, 538, 572, 636	15	25
S91G	407, 505, 528 (sh), 634	407, 505, 540 (sh), 580, 638	0	5
I9L/Y34N	408, 494 (sh), 523, 559 (sh), 633	418, 540, 575 (sh), 635	15	40
I9L/S91G	406, 504, 528 (sh), 635	406, 502, 538 (sh), 577, 639	0	0
Y34N/S91G	407, 504, 525 (sh), 634	408, 537, 577, 638	5	20
I9L/Y34N/S91G	407, 507, 525 (sh), 634	407, 505, 538, 576, 636	0	15
R32K/Y34N/N81S/S91G	407, 492 (sh), 536 (sh), 570 (sh), 638	411, 539, 578, 638	5	25

Peroxidase Studies. The oxidative dehalogenation of 2,4,6-trichlorophenols (TCP) to the corresponding 2,6-dichloro-1,4-benzoquinone (DCQ) as catalyzed by DHP was monitored as a function of H₂O₂ concentration by UV-visible spectroscopy at a fixed concentration of TCP¹². The two isoenzymes of DHP, A and B, exhibited differences in their kinetic parameters. DHP B has a 3-fold higher catalytic turnover (k_{cat}), and a 1.8-fold better overall catalytic efficiency (k_{cat}/K_m) compared to DHP A. Interestingly, the only single mutation that showed an increase in catalytic turnover was DHP A (I9L) (2.06 s⁻¹ vs. 0.90 s⁻¹ for WT DHP A; Table 2.5.). Every other single mutant of DHP showed a similar or a lower catalytic turnover as WT DHP A. To further highlight the importance of this position, every double mutant containing the I9L mutation also resulted increased catalytic turnover. Notably, DHP A (I9L/Y34N) exhibited the highest catalytic turnover (4.16 s⁻¹) of all mutants studied, a 4-fold increase from WT DHP A and a 1.5-fold increase from WT DHP B (2.72 s⁻¹). However, its catalytic efficiency (k_{cat}/K_m) was lower than WT DHP A due to a K_m value that was 6 times larger than WT DHP A (112 μ M vs. 19 μ M). All of the triple mutants containing the I9L mutation exhibited between a 2 and 3-fold increase in catalytic turnover (from 2.16 s⁻¹ to 2.96 s⁻¹) compared to DHP A and similar values to that observed for WT DHP B (2.72 s⁻¹). The

removal of I9L substitution from WT DHP B resulted in formation of DHP A (R32K/Y34N/N81S/S91G) (DHP B (L9I) and it displayed K_m and catalytic turnover nearly identical to WT DHP A ($15 \pm 2 \mu\text{M}$ vs $19 \pm 2 \mu\text{M}$ and 0.94 s^{-1} vs 0.90 s^{-1}). The triple mutants that contained the R32K mutation (I9L/R32K/Y34N, I9L/R32K/N81S, and I9L/R32K/S91G) exhibited lower K_m values than the other triple mutants, which in turn improved catalytic efficiency (k_{cat}/K_m) to be equivalent to WT DHP B ($0.081 \mu\text{M}^{-1} \text{ s}^{-1}$, $0.078 \mu\text{M}^{-1} \text{ s}^{-1}$, and $0.079 \mu\text{M}^{-1} \text{ s}^{-1}$, vs $0.083 \mu\text{M}^{-1} \text{ s}^{-1}$).

Comparing the k_{cat} values for the Y34N single mutant (0.73 s^{-1}) and the I9L/Y34N double mutant (4.16 s^{-1}) showed a nearly 6-fold difference. However, the I9L mutation only had an indirect contact to the distal side of the heme pocket through adjacent residues, such as Tyr16, Ile20, Phe115, Trp120, Phe60, Met 64, Val104, Tyr107 and Met108 (Figure 2.19). These results suggested that I9L has an effect on adjacent residues, which in turn, affect the sterics of the enzyme. The Y34N mutation removed one of the site for radical formation, which might lead to a different electron pathway in DHP and affected the observed kinetics of TCP oxidation.¹⁶

Table 2.5. Kinetic Data for the Oxidative Catalytic Reaction of TCP with DHP enzymes.

Enzyme	K_m (μM [H_2O_2])	k_{cat} (s^{-1})	k_{cat}/K_m ($\mu\text{M}^{-1} \text{s}^{-1}$)
WT DHP A	19 ± 2	0.90 ± 0.01	0.047
WT DHP B	33 ± 3	2.72 ± 0.05	0.083
I9L	53 ± 8	2.06 ± 0.06	0.039
R32K	16 ± 1	0.63 ± 0.01	0.039
Y34N	14 ± 1	0.73 ± 0.01	0.052
N81S	83 ± 9	0.87 ± 0.02	0.010
S91G	22 ± 3	0.40 ± 0.01	0.018
I9L/R32K	35 ± 6	1.80 ± 0.05	0.051
I9L/Y34N	112 ± 12	4.16 ± 0.12	0.037
I9L/N81S	39 ± 3	1.93 ± 0.03	0.050
I9L/S91G	43 ± 4	2.05 ± 0.02	0.048
R32K/Y34N	30 ± 1	1.13 ± 0.01	0.038
R32K/N81S	55 ± 4	0.83 ± 0.01	0.015
R32K/S91G	13 ± 2	0.55 ± 0.01	0.042
Y34N/N81S	30 ± 2	0.81 ± 0.01	0.027
Y34N/S91G	19 ± 1	1.11 ± 0.01	0.058
N81S/S91G	32 ± 5	0.96 ± 0.02	0.031
I9L/R32K/Y34N	33 ± 2	2.76 ± 0.03	0.081
I9L/R32K/N81S	35 ± 4	2.74 ± 0.04	0.078
I9L/R32K/S91G	29 ± 1	2.25 ± 0.01	0.079
I9L/Y34N/N81S	38 ± 2	2.31 ± 0.02	0.061
I9L/Y34N/S91G	51 ± 6	2.96 ± 0.07	0.058
I9L/N81S/S91G	38 ± 4	2.16 ± 0.04	0.057
R32K/Y34N/N81S/S91G (B L9I)	15 ± 2	0.94 ± 0.01	0.063

Reaction conditions: 0.5 μM DHP and 150 μM TCP, variable [H_2O_2] in 100 mM KPi (pH 7).

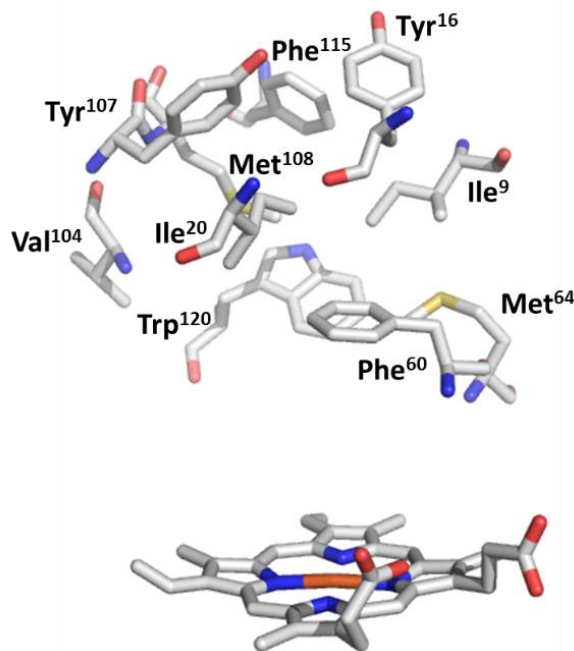


Figure 2.19. Ile9 and adjacent residues in WT DHP A (PDB: 4DWU).

Peroxygenase Studies. The hydrogen peroxide dependent oxidation of 5-Br-indole as catalyzed by DHP was monitored by HPLC (Table 2.6). A 2.2-fold difference in the percent conversion of 5-Br-indole was observed for WT DHP B (44.2%) when compared to isoenzyme A (20.6%).²² Single mutations at positions 9, 34, and 91 showed a similar peroxygenase activity as wild-type DHP A (22.2%, 19.0%, and 22.9% vs 20.6%, respectively), and in case of the mutations at positions 32 and 81 a significant decrease (10.8% and 11.0%) was noted. Every double mutant that did not contain the I9L mutation showed no significant variation in the percent conversion of 5-Br-indole (18.0-24.3%) when compared with wild type DHP A. Interesting results, however, were observed with the double mutants that contained the I9L mutation. All of the I9L double mutants (26.7 - 38.3%) showed an increase in peroxygenase activity when compared to WT DHP A (20.6%) with the exception of the I9L/N81S (21.9%) mutant. In particular, the I9L/Y34N mutant showed a near 2-fold increase in peroxygenase activity compared to WT DHP A (38.3% vs 20.6%), which puts it on a par with WT DHP B (44.2%). All of the triple mutants containing the I9L mutation exhibited a ~1.5- to 2-fold

increase over the corresponding double mutants, e.g. I9L/R32K/Y34N (37.3%) vs R32K/Y34N (21.4%). The I9L triple mutant which contained both proximal mutations (N81S and S91G) exhibited the least increase in peroxygenase activity (29.0%). However, the triple mutants I9L/Y34N/N81S (37.4%) and I9L/Y34N/S91G (36.0%) exhibited a peroxygenase activity similar to I9L/Y34N (38.3%) mutant. The peroxygenase activity of I9L/R32K/N81S and I9L/R32K/S91G was determined to be 33.6% and 34.5%, respectively. Removal of I9L substitution from WT DHP B resulted in DHP B (L9I) mutant. The peroxygenase activity of DHP B (L9I) was determined to be nearly identical to peroxygenase activity of WT DHP A (19.7% vs 20.6%).

The data obtained through site-directed mutagenesis of DHP A showed that an I9L substitution had a direct effect on the rate of peroxygenase activity. Why the substitution of a hydrophobic residue in isoleucine for its constitutional isomer in leucine would have such an effect remains a challenge to understand. Position 9 does not have a direct contact with the presumed haloindole binding pocket that is bordered, by residues Tyr16, Ile20, Phe115, Trp120, Phe60, Met64, Val104, Tyr107 and Met108.²¹ This suggests that steric interactions that arise from secondary effects on the residues that fall between the substrate binding pocket and position 9 maybe important factors in determining peroxygenase activity from their influences on the pocket.

Table 2.6. Enzyme-Catalyzed Reactivity of 5-Br-Indole with DHP Mutants.

Enzyme	5-Br-indole (%)
WT DHP A	20.6 ± 0.3
WT DHP B	44.2 ± 0.7
I9L	22.2 ± 0.3
R32K	10.8 ± 0.5
Y34N	19.0 ± 0.5
N81S	11.0 ± 0.3
S91G	22.9 ± 0.5
I9L/R32K	26.7 ± 0.3
I9L/Y34N	38.3 ± 0.5
I9L/N81S	21.9 ± 0.2
I9L/S91G	28.5 ± 0.5
R32K/Y34N	21.4 ± 0.5
R32K/N81S	18.0 ± 0.7
R32K/S91G	23.1 ± 1.0
Y34N/N81S	24.3 ± 1.0
Y34N/S91G	23.9 ± 0.3
N81S/S91G	21.5 ± 0.6
I9L/R32K/Y34N	37.3 ± 0.3
I9L/R32K/N81S	33.6 ± 0.7
I9L/R32K/S91G	34.5 ± 0.1
I9L/Y34N/N81S	37.4 ± 0.4
I9L/Y34N/S91G	36.0 ± 0.7
I9L/N81S/S91G	29.0 ± 0.1
R32K/Y34N/N81S/S91G (B L9I)	19.7 ± 0.4

Reaction Conditions: 10 μ M DHP , 500 μ M of 5-Br-indole, 500 μ M of H₂O₂, 5% MeOH in 100 mM KP_i (v/v) at pH 7, 25 °C, 5 min reaction.

Stopped-Flow UV-visible Studies. Formation of DHP transient species was investigated by single-mixing stopped-flow UV-visible spectroscopy at pH 7. A ferric solution of DHP was rapidly mixed (2 ms) with H₂O₂ to observe a formation of Compound ES. Compound ES is a ferryl-containing DHP intermediate with a radical formed on the protein moiety of the enzyme based on previous publications^{10-12, 30, 49} and comparison to known Fe(IV)-oxo species, containing hemoproteins¹¹ (Table 2.7). The rate constants (k_{obs}) of this

pseudo first order reaction for formation of Compound ES were linearly dependent on H₂O₂ concentration^{11, 12, 16}. In the absence of the substrate and excess of H₂O₂, Compound ES decays to a more stable specie Compound RH (*reversible heme*)^{11, 13} (Table 2.8).

Spectroscopic features of Compound ES of DHP A mutants formed by single, double and triple amino acid substitutions (I9L, Y34N, and S91G) closely resemble the spectroscopic features of Compound ES in WT DHP A with the exception of DHP A (S91G). Compound ES of DHP A (S91G) and DHP B (L9I) had similar spectroscopic features to Compound ES of WT DHP B. The bimolecular rate constants of Compound ES formation did not show any significant variation in the mutants tested. DHP A (I9L) and DHP A (Y34N) displayed rate of Compound ES formation similar to WT DHP B ($3.645 \times 10^4 \text{ M}^{-1} \text{ s}^{-1}$ and $3.496 \times 10^4 \text{ M}^{-1} \text{ s}^{-1}$ vs $3.504 \times 10^4 \text{ M}^{-1} \text{ s}^{-1}$). DHP A (S91G) showed a slight decrease in the rate compared to WT DHP A ($1.728 \times 10^4 \text{ M}^{-1} \text{ s}^{-1}$ vs $2.220 \times 10^4 \text{ M}^{-1} \text{ s}^{-1}$). Only DHP A (I9L/Y34N) double mutant displayed rate compatible to WT DHP B ($3.387 \times 10^4 \text{ M}^{-1} \text{ s}^{-1}$ vs $3.504 \times 10^4 \text{ M}^{-1} \text{ s}^{-1}$). The double mutants DHP A (I9L/S91G) and DHP A (Y34N/S91G) possessed rate similar to WT DHP A ($2.381 \times 10^4 \text{ M}^{-1} \text{ s}^{-1}$ and $2.431 \times 10^4 \text{ M}^{-1} \text{ s}^{-1}$ vs $2.220 \times 10^4 \text{ M}^{-1} \text{ s}^{-1}$). The triple mutant DHP A (I9L/Y34N/S91G) displayed the 1.7-fold increase in rate of formation of Compound ES compared to WT DHP B ($5.924 \times 10^4 \text{ M}^{-1} \text{ s}^{-1}$ vs $3.504 \times 10^4 \text{ M}^{-1} \text{ s}^{-1}$). Interestingly, the DHP B (L9I) mutant displayed a decrease in the rate compared to WT DHP B ($2.258 \times 10^4 \text{ M}^{-1} \text{ s}^{-1}$ vs $3.504 \times 10^4 \text{ M}^{-1} \text{ s}^{-1}$), which is similar to WT DHP A ($2.220 \times 10^4 \text{ M}^{-1} \text{ s}^{-1}$). This result suggests that I9L mutation has a critical effect on rate constant of Compound ES.

Spectroscopic features of Compound RH formed by various DHP A mutants were significantly different from each other and did not resemble Compound RH formed by WT DHP A and WT DHP B. The rate of formation of Compound RH did not show any significant variation from WT DHP A and WT DHP B with the exception of DHP A (I9L/Y34N). DHP A (I9L/Y34N) displayed a 4.7-fold decrease in the rate constant of Compound RH formation compared to WT DHP B ($6.07 \times 10^{-3} \text{ s}^{-1}$ vs $2.857 \times 10^{-2} \text{ s}^{-1}$). Compound RH is unable to form high-valent active intermediates, and possesses 6-fold lower reactivity with TCP as a substrate compared to WT DHP A.¹¹ The decrease in the rate of formation of Compound RH could

explain the unusually high catalytic activity of DHP A (I9L/Y34N) with TCP compared to WT DHP B (4.16 s^{-1} vs 2.72 s^{-1}).

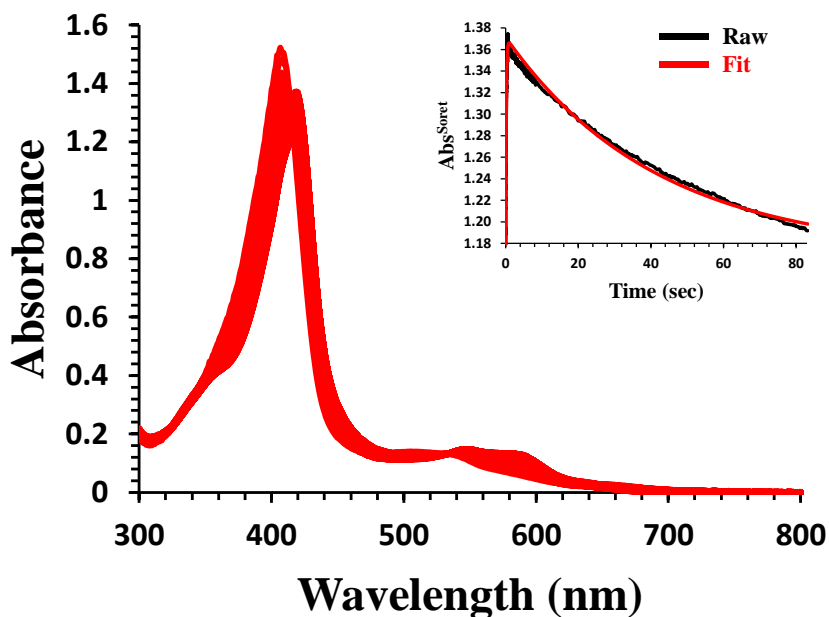


Figure 2.20. Reference stopped-flow UV-visible spectra of DHP A (I9L/Y34N/S91G) ($10 \mu\text{M}$) reacting with 10-fold excess of H_2O_2 at pH 7 (900 scans over 83 s); *inset*, the single wavelength (419 nm) dependence of time obtained from the raw spectra and its fit with a superposition of the calculated spectra components.

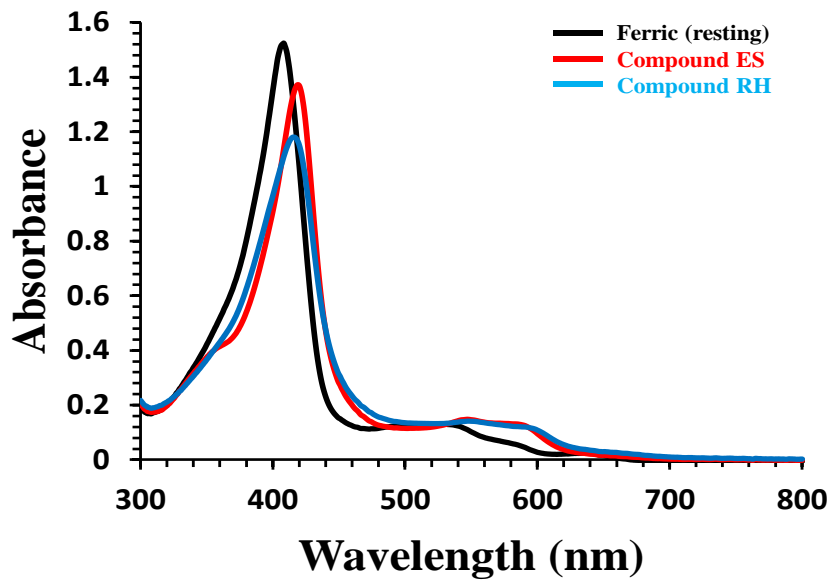


Figure 2.21. Reference calculated spectra of the three reaction components derived from the SVD analysis of data from **Figure 2.20**: ferric heme state (black), Compound ES (red) and Compound RH (blue).

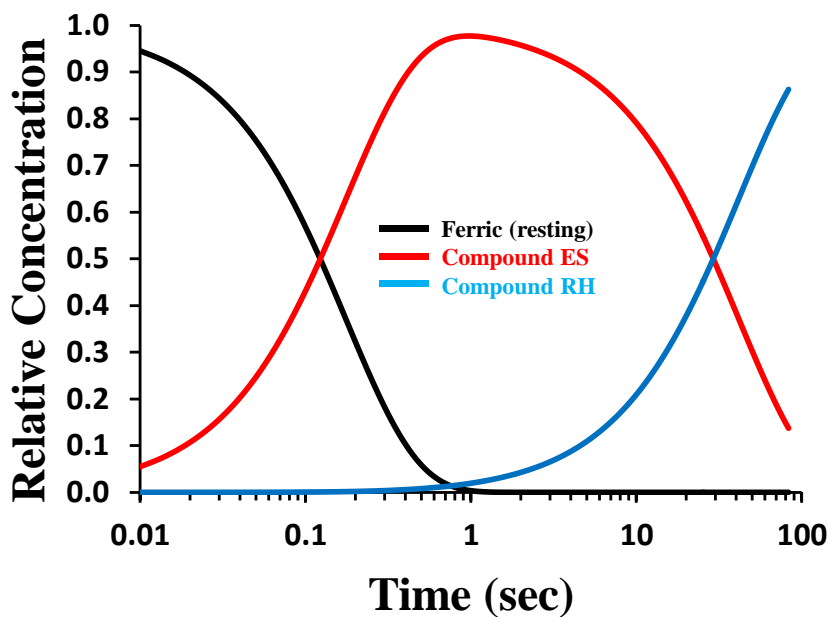


Figure 2.22. Reference time dependences of the relative concentrations for the three components as shown in the **Figure 2.21** determined by fitting the spectra set in **Figure 2.20**

Table 2.7. UV-visible spectroscopic features and rate of formation of Compound ES in DHP A and DHP B variants obtained with single mix stopped-flow experiment at pH 7.

Enzyme	k_{obs} ($\text{M}^{-1} \text{s}^{-1}$)	Spectroscopic Features
WT DHP A	$(2.220 \pm 0.066) \times 10^4$	420, 545, 587
WT DHP B	$(3.504 \pm 0.025) \times 10^4$	415, 543, 585
I9L	$(3.645 \pm 0.079) \times 10^4$	420, 547, 587
Y34N	$(3.496 \pm 0.024) \times 10^4$	419, 545, 588
S91G	$(1.728 \pm 0.014) \times 10^4$	416, 544, 585
I9L/Y34N	$(3.387 \pm 0.102) \times 10^4$	419, 544, 585
I9L/S91G	$(2.381 \pm 0.025) \times 10^4$	420, 546, 588
Y34N/S91G	$(2.431 \pm 0.017) \times 10^4$	420, 547, 586, 638 (sh)
I9L/Y34N/S91G	$(5.924 \pm 0.124) \times 10^4$	419, 546, 587
R32K/Y34N/N81S/S91G (B L9I)	$(2.258 \pm 0.020) \times 10^4$	415, 543, 587, 638

Table 2.8. UV-visible spectroscopic features and rate of formation of Compound RH in DHP A and DHP B variants obtained with single mix stopped-flow experiment at pH 7.

Enzyme	k_{obs} (s^{-1})	Spectroscopic Features
WT DHP A	$(1.888 \pm 0.122) \times 10^{-2}$	413, 536, 575 (sh)
WT DHP B	$(2.857 \pm 0.168) \times 10^{-2}$	410, 539, 586 (sh)
I9L	$(2.011 \pm 0.035) \times 10^{-2}$	412, 532, 570 (sh)
Y34N	$(3.038 \pm 0.047) \times 10^{-2}$	417, 545, 590 (sh)
S91G	$(3.951 \pm 0.113) \times 10^{-2}$	409, 502, 538 (sh), 576 (sh)
I9L/Y34N	$(6.07 \pm 0.20) \times 10^{-3}$	405, 446 (sh), 477 (sh), 523 (sh), 558 (sh), 613
I9L/S91G	$(3.128 \pm 0.043) \times 10^{-2}$	409, 536 (sh), 634
Y34N/S91G	$(2.756 \pm 0.291) \times 10^{-2}$	416, 544, 587 (sh), 636 (sh)
I9L/Y34N/S91G	$(2.414 \pm 0.010) \times 10^{-2}$	416, 549, 594
R32K/Y34N/N81S/S91G	$(2.496 \pm 0.046) \times 10^{-2}$	410, 539, 579 (sh), 639

5-Br-indole Binding Studies. To further examine the effect of the I9L substitution on peroxxygenase activity, substrate binding studies were performed on the WT enzyme and three I9 mutants to determine if the observed differences in 5-Br-indole conversion could be explained by differences in substrate binding affinity. WT DHP A had a very weak binding affinity ($>1400 \mu\text{M}$) to 5-Br-indole and 5-I-indole, which was reflected by a lack of measurable

K_d value (Table 2.6). However, the DHP A (I9L) mutant exhibited a 5-Br-indole binding affinity equivalent to DHP B (145 μM vs. 150 μM ²²). The DHP A (I9L/Y34N) double mutant also showed a similar trend with improved binding affinity compared to DHP A (175 μM vs. >1400 μM).

Additional DHP A mutants were generated utilizing a range of hydrophobic residues (Val, Ala, and Gly). Out of three mutants, only the I9V mutant was expressed and purified successfully. DHP A (I9V) was found to have a weak binding affinity (>1400 μM) for both 5-Br-indole and 5-I-indole, an observation that was reflected by a low 5-Br-indole conversion percentage.

Table 2.9. Dissociation Constants for 5-Br-indole and 5-I-indole.

Enzyme	5-Br-indole (%) ^a	K_d (5-Br-indole) ^b	K_d (5-I-indole) ^b
WT DHP A	20.6 \pm 0.3	> 1400	> 1400
WT DHP B	44.2 \pm 0.7	150 \pm 10	62 \pm 10
I9L	22.2 \pm 0.3	145 \pm 7	96 \pm 5
I9L/Y34N	38.3 \pm 0.5	175 \pm 6	88 \pm 9
I9V	17.2 \pm 0.2	> 1400	> 1400
R32K/Y34N/N81S/S91G (B L9I)	19.7 \pm 0.4	> 1400	> 1400

^aReaction conditions were as described in Table 2.3. ^bBinding assay conditions: 10 μM DHP in 10% MeOH/100 mM KP_i (v/v) at pH 7.

Resonance Raman Studies. Resonance Raman spectra were collected of 100 μM ferric DHP A (I9L) (Figure 2.9) and DHP A (I9L/Y34N) (Figure 2.10) in the presence of 1 mM 5-Br-indole or 5-I-indole in 100 mM KP_i containing 10% MeOH (v/v) at pH 7, and compared to previously reported spectra of WT DHP B (same conditions)²², and WT DHP A (100 mM KP_i and 10% MeOH/100 mM KP_i (v/v))³⁵. In aqueous buffer WT DHP A, WT DHP B, DHP A (I9L) and DHP A (I9L/Y34N) are a mixture of five-coordinated high spin (5cHS, ν_3 at 1494 cm^{-1} , and ν_2 at 1569 cm^{-1}) and six-coordinated high spin (6cHS, ν_3 at 1477 cm^{-1} , and ν_2 at 1563 cm^{-1}) hemes. These results align with the observations of relative high spin heme populations

obtained by comparing UV-vis ratios of A_{Soret}/A_{380} and A_{614}/A_{645} . In addition, DHP A (I9L/Y34N) mixture contained some oxyferrous form of the enzyme indicated by increased intensity at 1504 cm^{-1} , which clarifies the deviations observed in the UV-vis spectrum. However, all of the enzymes are nearly 100% 6cHS heme in 10% MeOH, with H_2O bound to Fe in the sixth (axial) position. Presumably, this arose from a destabilization of a distal histidine (His55) in the solvent exposed “open” conformation in the 10% MeOH buffer solution.²² Similar to WT DHP B, both mutants displayed a decrease in 6cHS core size marker band frequencies for haloindole bound DHP compared to only DHP in buffer solution. These results are consistent with previously reported observations that both 4-halophenols⁴³ and 5-haloindoles⁴³ bind in the distal pocket above the heme iron and forcing the distal histidine (His55) into “open” conformation.^{34, 39} This destabilizes an iron-bound water due to removed hydrogen bonding with His55, and an increase in the 5cHS heme population is observed.

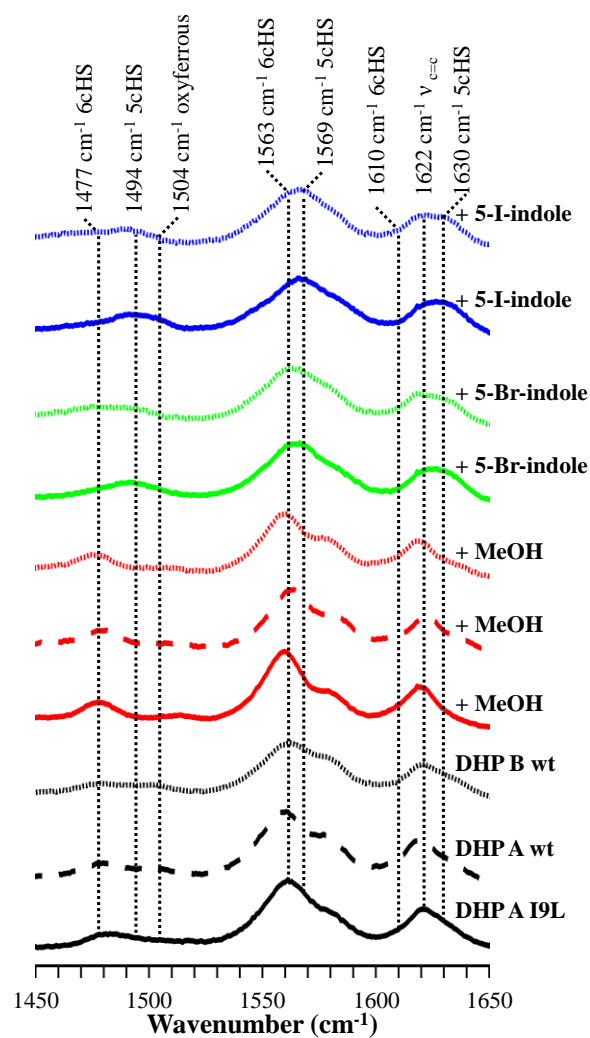


Figure 2.23. Resonance Raman spectra of DHP A (I9L) (solid line), WT DHP A (dashed line), WT DHP B (dotted line) in 100 mM KP_i (black), in 10% MeOH/100 mM KP_i (v/v) (red), 1 mM 5-Br-indole (green) and 5-I-indole (blue) in 10% MeOH/100 mM KP_i (v/v) at pH 7.

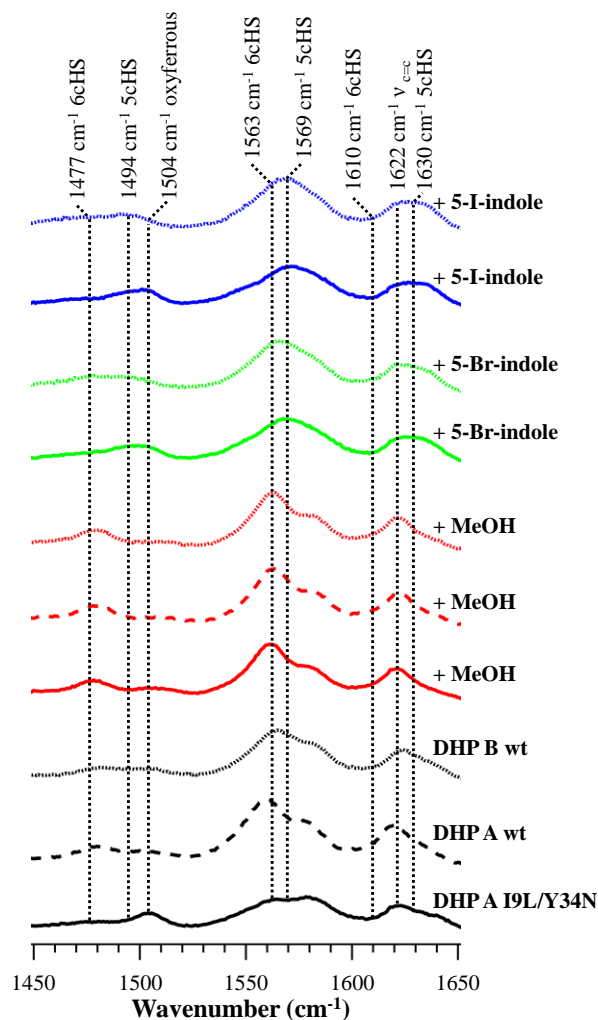


Figure 2.24. Resonance Raman spectra of DHP A (I9L/Y34N) (solid line), WT DHP A (dashed line), WT DHP B (dotted line) in 100 mM KP_i (black), in 10% MeOH/100 mM KP_i (v/v) (red), 1 mM 5-Br-indole (green) and 5-I-indole (blue) in 10% MeOH/100 mM KP_i (v/v) at pH 7.

Conclusions

The structure-function relationships of DHP were probed using 21 mutants of DHP A. Activity assays (peroxidase and peroxygenase) and binding studies elucidated the I9L mutation to be a key determinant in the structure-function relationships between isoenzymes A and B. The I9L containing mutants exhibited similar binding affinities of 5-Br-indole and 5-I-indole,

as DHP B. In addition, the I9L mutant showed a synergistically beneficial effect with other single and double mutants. These findings were unexpected due to location of I9L mutation in relation to distal pocket. Position 9 is located in a hydrophobic region of the enzyme and does not have a direct contact with heme pocket. However, it may have an effect on the pocket through steric interactions with adjacent amino acid residues.

Examination of Q-bands in UV-vis spectra of mutants of DHP A presented an interesting competing effects involving I9L, Y34N and S91G mutations. The addition of Y34N substitution increases the rate of reduction of ferric form of the enzyme resulting in increase of oxyferrous form of the enzyme. However, addition of I9L substitution to Y34N containing mutants results in minor increase in five-coordinate ferric heme population and a subsequent decrease of oxyferrous form of the enzyme. Furthermore, addition of S91G substitution to Y34N containing mutant is able to virtually completely revert the effect of Y34N mutation and prevent increased reduction of the ferric enzyme to oxyferrous form.

References:

1. Woodin, S. A.; Walla, M. D.; Lincoln, D. E. Occurrence of brominated compounds in soft-bottom benthic organisms. *J. Exp. Mar. Biol. Ecol.* **1987**, *107*, 209-217.
2. Woodin, S. A. Recruitment of Infauna: Positive or Negative Cues? *Amer. Zool.* **1991**, *31* (6), 797-807.
3. Gribble, G. W. The diversity of naturally occurring organobromine compounds. *Chem. Soc. Rev.* **1999**, *28*, 335-346.
4. Gribble, G. W. The natural production of organobromine compounds. *Environ. Sci. Pollut. Res. Int.* **2000**, *7* (1), 37-49.
5. Han, K.; Woodin, S. A.; Lincoln, D. E.; Fielman, K. T.; Ely, B. Amphitrite ornata, a marine worm, contains two dehaloperoxidase genes. *Mar Biotechnol (NY)* **2001**, *3* (3), 287-92.
6. Chen, Y. P.; Woodin, S. A.; Lincoln, D. E.; Lovell, C. R. An Unusual Dehalogenating Peroxidase from the Marine Terebellid Polychaete *Amphitrite ornata*. *J. Biol. Chem.* **1996**, *271* (9), 4609-4612.
7. Lebioda, L.; LaCount, M. W.; Zhang, E.; Chen, Y. P.; Han, K.; Whitton, M. M.; Lincoln, D. E.; Woodin, S. A. An enzymatic globin from a marine worm. *Nature* **1999**, *401*, 445.
8. Osborne, R. L.; Taylor, L. O.; Han, K. P.; Ely, B.; Dawson, J. H. Amphitrite ornata dehaloperoxidase: enhanced activity for the catalytically active globin using MCPBA. *Biochem Biophys Res Commun* **2004**, *324* (4), 1194-8.
9. Weber, R. E.; Mangum, C.; Steinman, H.; Bonaventura, C.; Sullivan, B.; Bonaventura, J. Hemoglobins of two terebellid polychaetes: *Enoplobranchus sanguineus* and *Amphitrite ornata*. *Comp. Biochem. Physiol.* **1977**, *56A*, 179-187.
10. Belyea, J. L.; Gilvey, L. B.; Davis, M. F.; Godek, M.; Sit, T. L.; Lommel, S. A.; Franzen, S. Enzyme Function of the Globin Dehaloperoxidase from *Amphitrite ornata* Is Activated by Substrate Binding. *Biochemistry* **2005**, *44* (48), 15637-15644.
11. Feducia, J.; Dumariéh, R.; Gilvey, L. B.; Smirnova, T.; Franzen, S.; Ghiladi, R. A. Characterization of dehaloperoxidase compound ES and its reactivity with trihalophenols. *Biochemistry* **2009**, *48* (5), 995-1005.

12. D'Antonio, J.; D'Antonio, E. L.; Thompson, M. K.; Bowden, E. F.; Franzen, S.; Smirnova, T.; Ghiladi, R. A. Spectroscopic and Mechanistic Investigations of Dehaloperoxidase B from *Amphitrite ornata*. *Biochemistry* **2010**, *49* (31), 6600-16.
13. Thompson, M.; Franzen, S.; Ghiladi, R. A.; Reeder, B. J.; Svistunenko, D. A. Compound ES of Dehaloperoxidase Decays via Two Alternative Pathways Depending on the Conformation of the Distal Histidine. *J Am Chem Soc* **2010**, *132* (49), 17501-17510.
14. D'Antonio, E. L.; D'Antonio, J.; de Serrano, V.; Gracz, H.; Thompson, M. K.; Ghiladi, R. A.; Bowden, E. F.; Franzen, S. Functional consequences of the creation of an Asp-His-Fer triad in a 3/3 globin. *Biochemistry* **2011**, *50* (44), 9664-80.
15. D'Antonio, J.; Ghiladi, R. A. Reactivity of deoxy- and oxyferrous dehaloperoxidase B from *Amphitrite ornata*: identification of compound II and its ferrous-hydroperoxide precursor. *Biochemistry* **2011**, *50* (27), 5999-6011.
16. Dumarieh, R.; D'Antonio, J.; Deliz-Liang, A.; Smirnova, T.; Svistunenko, D. A.; Ghiladi, R. A. Tyrosyl radicals in dehaloperoxidase: how nature deals with evolving an oxygen-binding globin to a biologically relevant peroxidase. *J Biol Chem* **2013**, *288* (46), 33470-82.
17. Osborne, R. L.; Sumithran, S.; Coggins, M. K.; Chen, Y. P.; Lincoln, D. E.; Dawson, J. H. Spectroscopic characterization of the ferric states of *Amphitrite ornata* dehaloperoxidase and *Notomastus lobatus* chloroperoxidase: His-ligated peroxidases with globin-like proximal and distal properties. *J Inorg Biochem* **2006**, *100* (5-6), 1100-8.
18. Osborne, R. L.; Coggins, M. K.; Raner, G. M.; Walla, M.; Dawson, J. H. The mechanism of oxidative halophenol dehalogenation by *Amphitrite ornata* dehaloperoxidase is initiated by H₂O₂ binding and involves two consecutive one-electron steps: role of ferryl intermediates. *Biochemistry* **2009**, *48* (20), 4231-8.
19. Davydov, R.; Osborne, R. L.; Shanmugam, M.; Du, J.; Dawson, J. H.; Hoffman, B. M. Probing the Oxyferrous and Catalytically Active Ferryl States of *Amphitrite ornata* Dehaloperoxidase by Cryoreduction and EPR/ENDOR Spectroscopy. Detection of Compound I. *J Am Chem Soc* **2010**, *132* (42), 14995-15004.
20. Du, J.; Sono, M.; Dawson, J. H. Functional switching of *Amphitrite ornata* dehaloperoxidase from O₂-binding globin to peroxidase enzyme facilitated by halophenol substrate and H₂O₂. *Biochemistry* **2010**, *49* (29), 6064-9.
21. de Serrano, V.; D'Antonio, J.; Franzen, S.; Ghiladi, R. A. Structure of dehaloperoxidase B at 1.58 Å resolution and structural characterization of the AB dimer from *Amphitrite ornata*. *Acta Crystallogr D Biol Crystallogr* **2010**, *66* (Pt 5), 529-38.

22. Barrios, D. A.; D'Antonio, J.; McCombs, N. L.; Zhao, J.; Franzen, S.; Schmidt, A. C.; Sombers, L. A.; Ghiladi, R. A. Peroxygenase and Oxidase Activities of Dehaloperoxidase-Hemoglobin from Amphitrite ornata. *J Am Chem Soc* **2014**.
23. Franzen, S.; Thompson, M. K.; Ghiladi, R. A. The dehaloperoxidase paradox. *Biochim Biophys Acta* **2012**, 1824 (4), 578-88.
24. Mangum, C.; Woodin, B. R.; Bonaventura, C.; Sullivan, B.; Bonaventura, J. The role of coelomic and vascular hemoglobin in the annelid family terebellidae. *Comp. Biochem. Physiol.* **1975**, 51A, 281-294.
25. Chiancone, E.; Brenowitz, M.; Ascoli, F.; Bonaventura, C.; Bonaventura, J. *Amphitrite ornata* erythrocyruorin. I. Structural properties and characterization of subunit interactions. *Biochim Biophys Acta* **1980**, 623, 146-162.
26. Chiancone, E.; Ferruzzi, G.; Bonaventura, C.; Bonaventura, J. *Amphitrite ornata* erythrocyruorin II. Molecular controls of function. *Biochim Biophys Acta* **1981**, 670, 84-92.
27. Roach, M. P.; P., C. Y.; Woodin, S. A.; Lincoln, D. E.; Dawson, J. H. Notomastus lobatus Chloroperoxidase and Amphitrite ornata Dehaloperoxidase Both Contain Histidine as Their Proximal Heme Iron Ligand. *Biochemistry* **1997**, 36 (8), 2197-2202.
28. LaCount, M. W.; Zhang, E.; Chen, Y. P.; Han, K.; Whitton, M. M.; Lincoln, D. E.; Woodin, S. A.; Lebioda, L. The crystal structure and amino acid sequence of dehaloperoxidase from Amphitrite ornata indicate common ancestry with globins. *J Biol Chem* **2000**, 275 (25), 18712-6.
29. Du, J.; Huang, X.; Sun, S.; Wang, C.; Lebioda, L.; Dawson, J. H. Amphitrite ornata dehaloperoxidase (DHP): investigations of structural factors that influence the mechanism of halophenol dehalogenation using "peroxidase-like" myoglobin mutants and "myoglobin-like" DHP mutants. *Biochemistry* **2011**, 50 (38), 8172-80.
30. Franzen, S.; Gilvey, L. B.; Belyea, J. L. The pH dependence of the activity of dehaloperoxidase from Amphitrite ornata. *Biochim Biophys Acta* **2007**, 1774 (1), 121-30.
31. de Serrano, V.; Chen, Z.; Davis, M. F.; Franzen, S. X-ray crystal structural analysis of the binding site in the ferric and oxyferrous forms of the recombinant heme dehaloperoxidase cloned from Amphitrite ornata. *Acta Crystallogr D Biol Crystallogr* **2007**, 63 (Pt 10), 1094-101.
32. Lo Conte, L.; Ailey, B.; Hubbard, T.; Brenner, S. E.; Murzin, A. G.; Chothia, C. SCOP: a Structural Classification of Proteins database. *Nuc. Ac. Res.* **2000**, 28 (1), 257-259.

33. Poulos, T. L.; Kraut, J. The Stereochemistry of Peroxidase Catalysis. *J. Biol. Chem.* **1980**, *255* (17), 8199-8205.
34. Plummer, A.; Thompson, M. K.; Franzen, S. Role of polarity of the distal pocket in the control of inhibitor binding in dehaloperoxidase-hemoglobin. *Biochemistry* **2013**, *52* (13), 2218-27.
35. Zhao, J.; de Serrano, V.; Dumariéh, R.; Thompson, M.; Ghiladi, R. A.; Franzen, S. The role of the distal histidine in H₂O₂ activation and heme protection in both peroxidase and globin functions. *J Phys Chem B* **2012**, *116* (40), 12065-77.
36. Poulos, T. L. Thirty years of heme peroxidase structural biology. *Arch Biochem Biophys* **2010**, *500* (1), 3-12.
37. Battistuzzi, G.; Bellei, M.; Bortolotti, C. A.; Sola, M. Redox properties of heme peroxidases. *Arch Biochem Biophys* **2010**, *500* (1), 21-36.
38. Matsui, T.; Ozaki, S. i.; Liong, E.; Phillips, G. N.; Watanabe, Y. Effects of the Location of Distal Histidine in the Reaction of Myoglobin with Hydrogen Peroxide. *J. Biol. Chem.* **1999**, *274* (5), 2838-2844.
39. Chen, Z.; de Serrano, V.; Betts, L.; Franzen, S. Distal histidine conformational flexibility in dehaloperoxidase from *Amphitrite ornata*. *Acta Crystallogr D Biol Crystallogr* **2009**, *65* (Pt 1), 34-40.
40. D'Antonio, E. L.; Bowden, E. F.; Franzen, S. Thin-layer spectroelectrochemistry of the Fe(III)/Fe(II) redox reaction of dehaloperoxidase-hemoglobin. *J. Electroanal. Chem.* **2012**, *668*, 37-43.
41. Sono, M.; Roach, M. P.; Coulter, E. D.; Dawson, J. H. Heme-Containing Oxygenases. *Chem. Rev.* **1996**, *96* (7), 2841-2887.
42. Meunier, B.; de Visser, S. P.; Shaik, S. Mechanism of Oxidation Reactions Catalyzed by Cytochrome P450 Enzymes. *Chem. Rev.* **2004**, *104* (9), 3947-3980.
43. Thompson, M. K.; Davis, M. F.; de Serrano, V.; Nicoletti, F. P.; Howes, B. D.; Smulevich, G.; Franzen, S. Internal binding of halogenated phenols in dehaloperoxidase-hemoglobin inhibits peroxidase function. *Biophys J* **2010**, *99* (5), 1586-95.
44. Nicoletti, F. P.; Thompson, M. K.; Howes, B. D.; Franzen, S.; Smulevich, G. New Insights into the Role of Distal Histidine Flexibility in Ligand Stabilization of Dehaloperoxidase-Hemoglobin from *Amphitrite ornata*. *Biochemistry* **2010**, *49* (9), 1903-1912.

45. Chenprakhon, P.; Sucharitakul, J.; Panijpan, B.; Chaiyen, P. Measuring Binding Affinity of Protein–Logan Interaction Using Spectrophotometer: Binding of Neutral Red to Riboflavin-Binding Protein. *J. Chem. Educ.* **2010**, *87* (8), 829-831.
46. Chouchane, S.; Giroto, S.; Kapetanaki, S.; Schelvis, J. P.; Yu, S.; Magliozzo, R. S. Analysis of heme structural heterogeneity in *Mycobacterium tuberculosis* catalase-peroxidase (KatG). *J Biol Chem* **2003**, *278* (10), 8154-62.
47. Ghiladi, R. A.; Medzihradzky, K. F.; Rusnak, F. M.; Ortiz de Montellano, P. R. Correlation between Isoniazid Resistance and Superoxide Reactivity in *Mycobacterium tuberculosis* KatG. *J Am Chem Soc* **2005**, *127* (38), 13428-13442.
48. Ghiladi, R. A.; Medzihradzky, K. F.; Ortiz de Montellano, P. R. Role of the Met–Tyr–Trp Cross-Link in *Mycobacterium tuberculosis* Catalase-Peroxidase (KatG) As Revealed by KatG(M255I). *Biochemistry* **2005**, *44* (46), 15093-15105.
49. Franzen, S.; Belyea, J. L.; Gilvey, L. B.; Davis, M. F.; Chaudhary, C. E.; Sit, T. L.; Lommel, S. A. Proximal Cavity, Distal Histidine, and Substrate Hydrogen-Bonding Mutations Modulate the Activity of *Amphitrite ornata* Dehaloperoxidase. *Biochemistry* **2006**, *45* (30), 9085-9094.